Electronic Supplementary Information (ESI) for Dalton Transactions

This journal is © The Royal Society of Chemistry 2019

Supporting Information For:

A recyclable post-synthetically modified Al(III) based metal-organic framework for fast and selective fluorogenic recognition of bilirubin in human biofluids

*Soutick Nandi and Shyam Biswas**

Department of Chemistry, Indian Institute of Technology Guwahati, Guwahati, 781039 Assam, India.

* Corresponding author. Tel: 91-3612583309, Fax: 91-3612582349.

E-mail address: sbiswas@iitg.ac.in.

Materials and Characterization Methods. All the required chemicals were purchased from commercial sources and used without purification. Fourier transform infrared (FT-IR) spectra were recorded with a Perkin Elmer Spectrum two FT-IR spectrometer in the range of 440-4000 cm^{-1} with KBr pellet. The below mentioned indications were employed for the characterization of the absorption bands: medium (m), weak (w), broad (br), very strong (vs), strong (s) and shoulder (sh). Ambient temperature X-Ray powder diffraction (XRPD) patterns were collected on a Bruker D2 Phaser X-ray diffractometer (30 kV, 10 mA) using Cu-*K*α (λ = 1.5406 Å) radiation. FE-SEM images were captured with a Zeiss (Zemini) scanning electron microscope. Thermogravimetric analyses (TGA) were collected under air atmosphere at a heating rate of 10 °C min^{-1} in a temperature region of 25-800 °C by employing a Netzsch STA-409CD thermal analyzer. Fluorescence emission behavior was recorded by a HORIBA JOBIN YVON Fluoromax-4 spectrofluorometer. The excitation wavelength (λ_{ex}) was 325 nm for all the fluorescence experiments. The nitrogen sorption isotherms were performed employing a Quantachrome Autosorb iQ-MP gas sorption analyzer at -196 °C. Prior to the sorption measurement, degassing of the material was performed at 120 °C for 12 h under dynamic vacuum. A Bruker Avance III 600 spectrometer was utilized for recording ^{1}H-NMR at 600 MHz. The mass spectrum (in ESI mode) was measured with an Agilent 6520 Q-TOF high-resolution mass spectrometer. Fluorescence lifetime measurements were performed by time correlated single-photon counting (TCSPC) method by an Edinburgh Instrument Life-Spec II instrument. The fluorescence decays were analyzed by reconvolution method using the FAST software provided by Edinburgh Instruments. Zeta potential was measured with a Zetasizer Nano ZS90 (model no. ZEN3690) instrument. X-ray photoelectron spectroscopy (XPS) measurement was carried out at room temperature using a custom-built near-ambient pressure photoelectron spectrometer (Prevac, Poland). It is equipped with an R3000HP analyser (Scienta) with a twin-anode source and a monochromatic (Al-Kα) X-ray source.

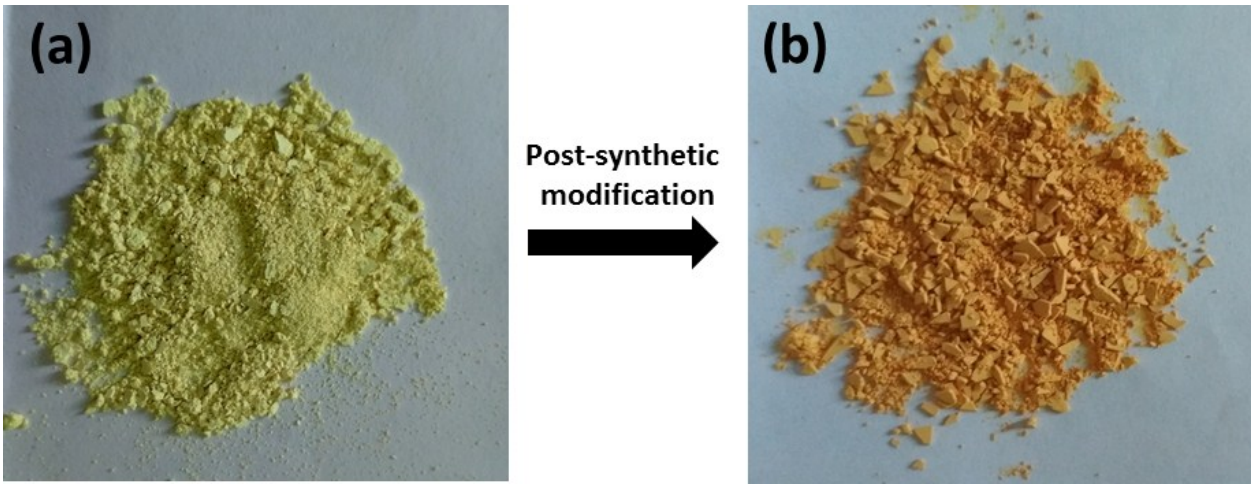

Figure S1. Digital images of **1-NH_2** (a) and **1-NH_2@THB** (b) in solid state.

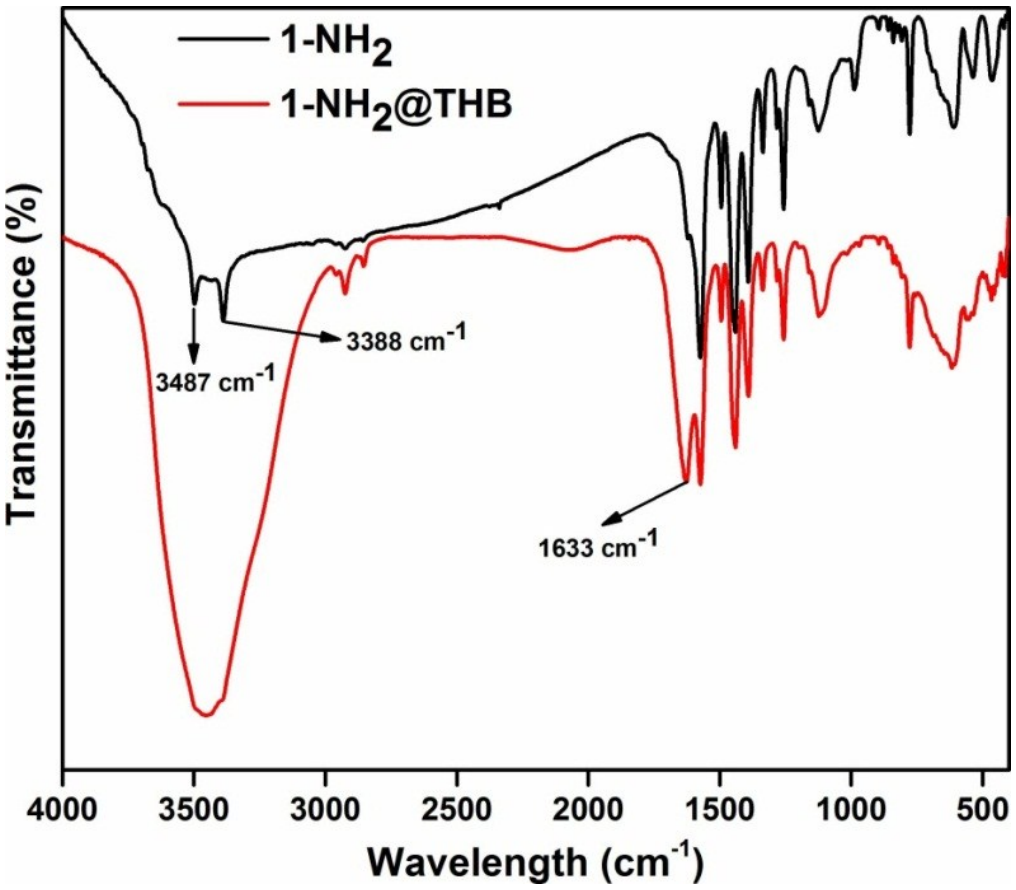

Figure S2. FT-IR spectra of **1-NH_2** (black) and **1-NH_2@THB** (red).

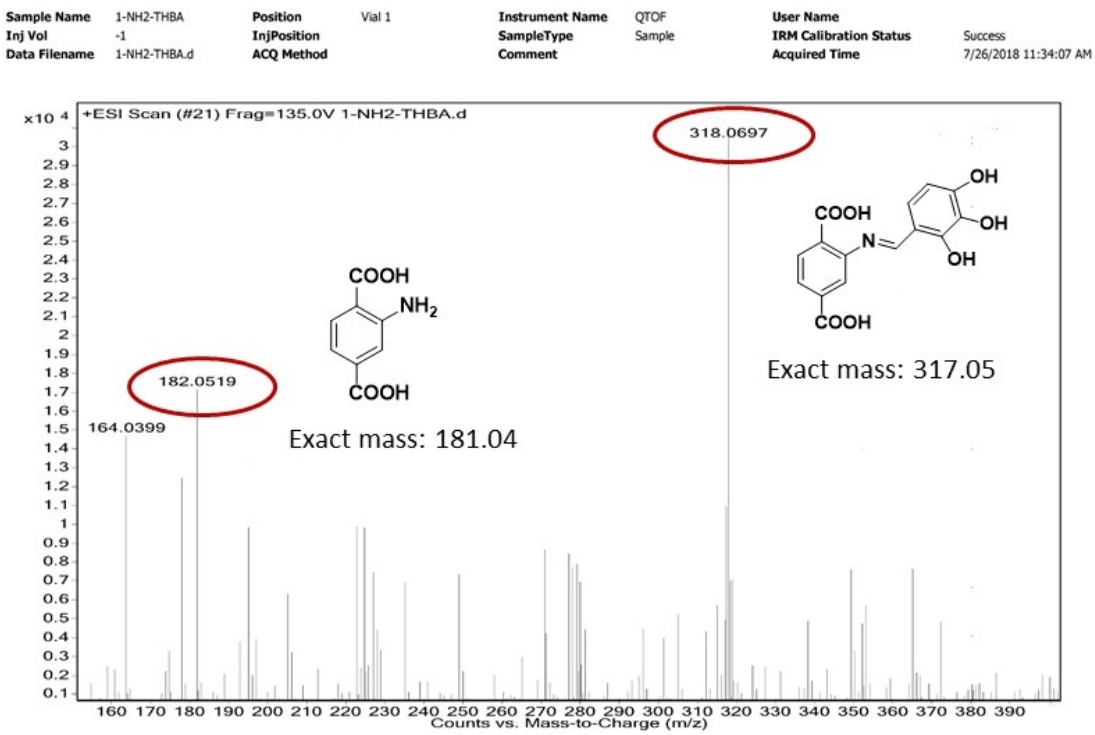

Figure S3. ESI-MS spectrum of the digested framework of **1-NH_2@THB** showing m/z (positive ion mode) peaks at 182.0519 and 318.0697, which correspond to $(M+H)^+$ ion (M = mass of ligands) of H_2BDC-NH_2 ligand and the imine-functionalized ligand, respectively. This spectrum further confirms the formation of imine bond. *Digestion protocol of the MOF sample for recording ESI-MS spectrum:* 10 mg of MOF sample was added to 1.0 mL of DMSO. To this solution, 1.0 mL of saturated K_3PO_4 (in H_2O) was added. After sonication for 5 min, the MOF sample was totally dissolved. The organic phase was separated and diluted with HPLC grade methanol for ESI-MS analysis.

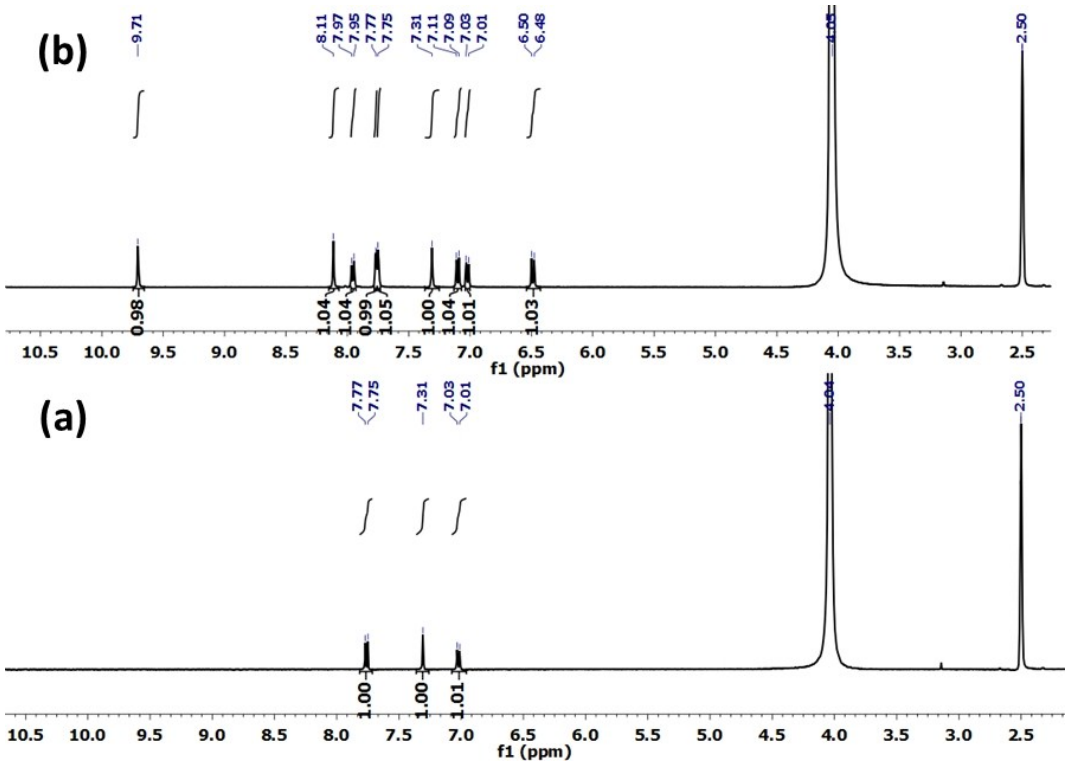

Figure S4. ^{1}H NMR spectra of (a) **1-NH_2** and (b) **1-NH_2@THB** after framework digestion in K_3PO_4/D_2O. The assignment of the NMR peaks for **1-NH_2@THB** was interpreted according to the presence of the new peaks observed for the phenyl and imine moiety. To calculate the percent of conversion, the aromatic proton peaks corresponding to H_2BDC-NH_2 ligand were set to an integration of 1 and all new peaks were integrated accordingly. For **1-NH_2@THB**, new peaks are all approx. ~1.04 with respect to aromatic protons of H_2BDC-NH_2 ligand, corresponding to a conversion of ~51%. *Digestion protocol of the MOF sample for recording NMR spectra:* 10 mg of each MOF sample was added to 400 µL of DMSO-d_6. To this solution, 200 µL of saturated K_3PO_4 in D_2O was added. After shaking for 5 min, the MOF sample was totally dissolved and the organic phase was analyzed by ^{1}H NMR spectroscopy immediately.

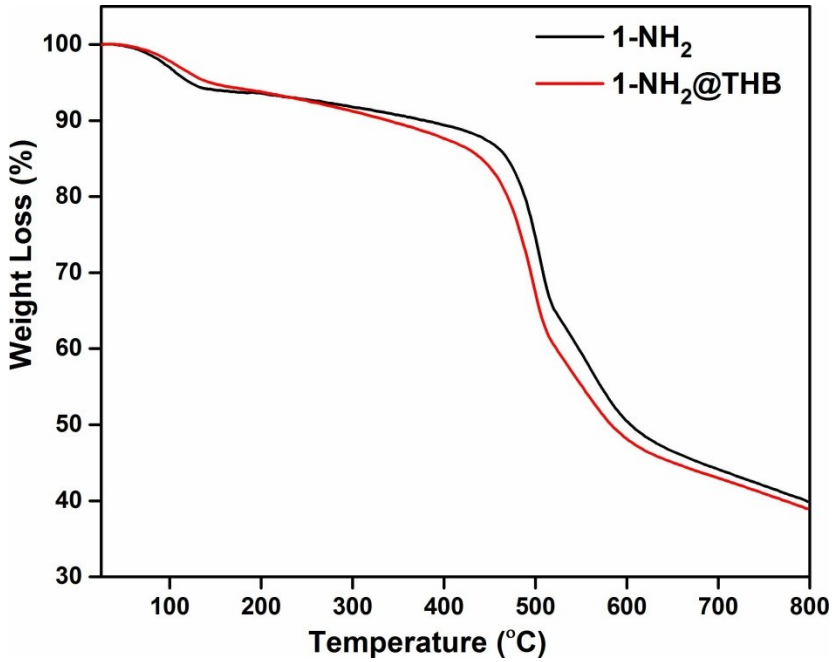

Figure S5. TG curves of **1-NH$_2$** and **1-NH$_2$@THB** recorded in the temperature range of 25-800 °C with a heating rate of 10 °C min^{-1}.

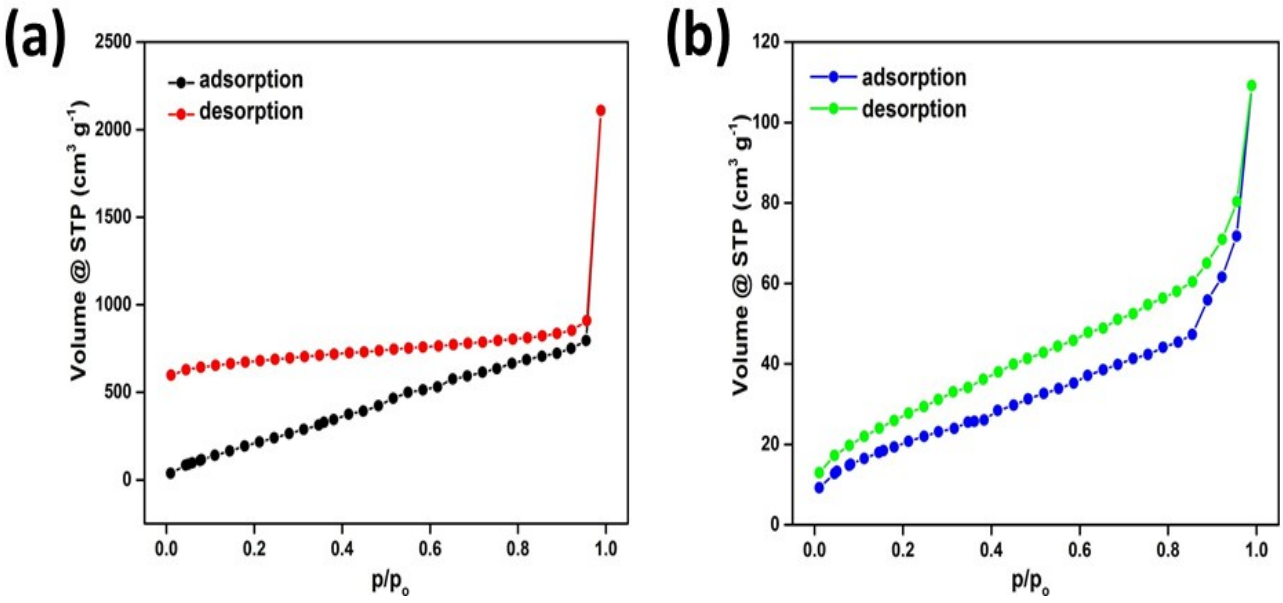

Figure S6. N_2 adsorption and desorption isotherms of **1-NH$_2$** (a) and **1-NH$_2$@THB** (b) recorded at –196 °C.

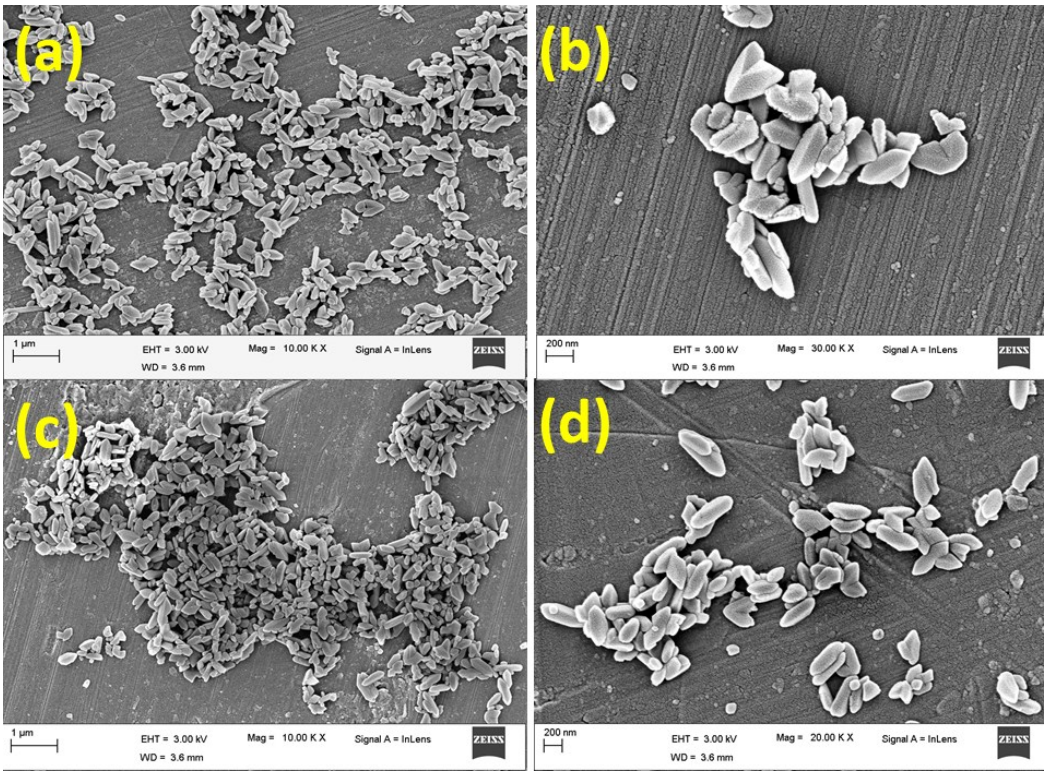

Figure S7. FE-SEM images of **1-NH$_2$** (a, b) and **1-NH$_2$@THB** (c, d).

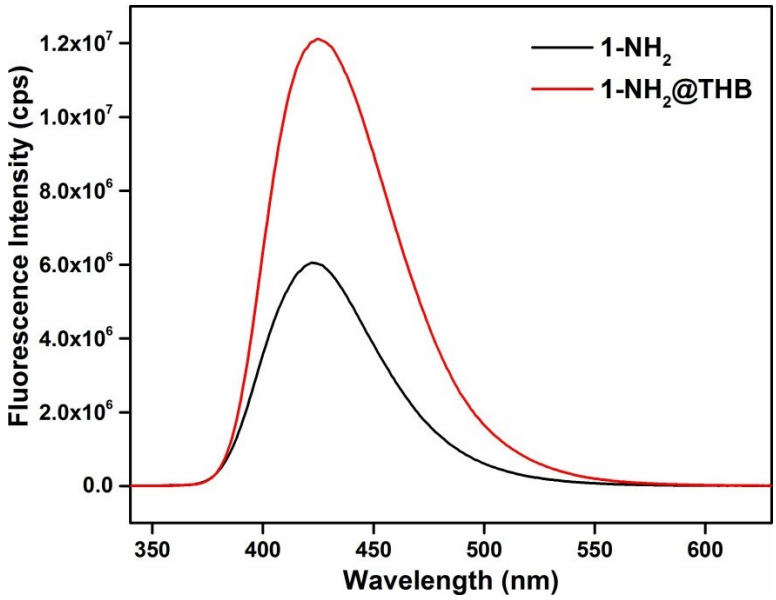

Figure S8. Fluorescence emission spectra of **1-NH$_2$** (black) and **1-NH$_2$@THB** (red).

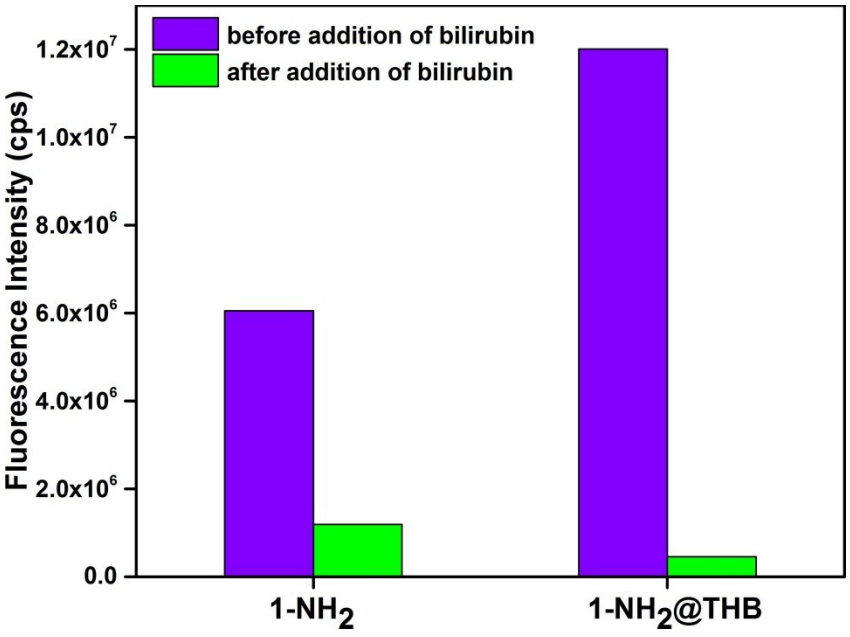

Figure S9. Fluorescence emission intensity of **1-NH_2** and **1-NH_2@THB** before and after addition of bilirubin.

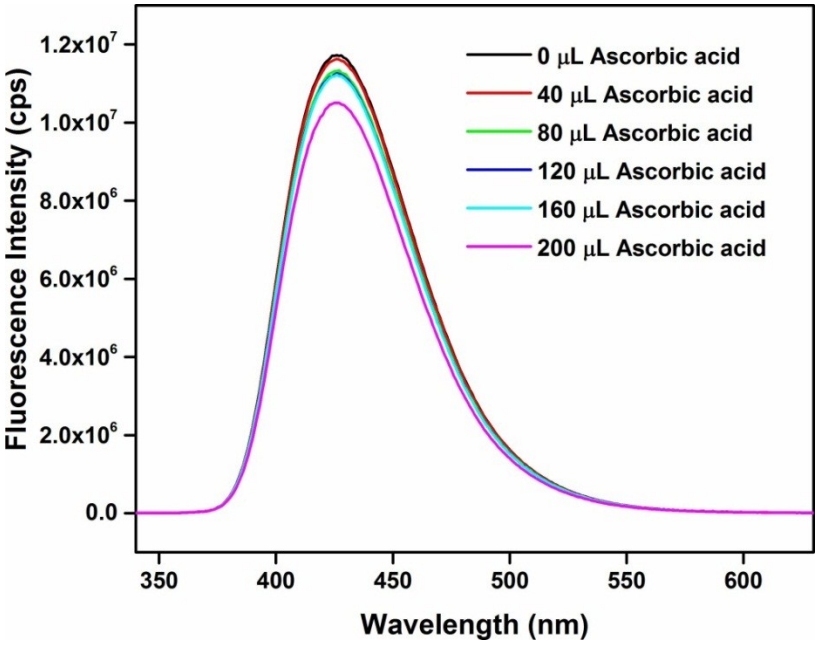

Figure S10. Change in the fluorescence emission intensity of **1-NH_2@THB** upon incremental addition of 1 mM ascorbic acid solution (λ_{ex}= 325 nm and λ_{em}= 429 nm).

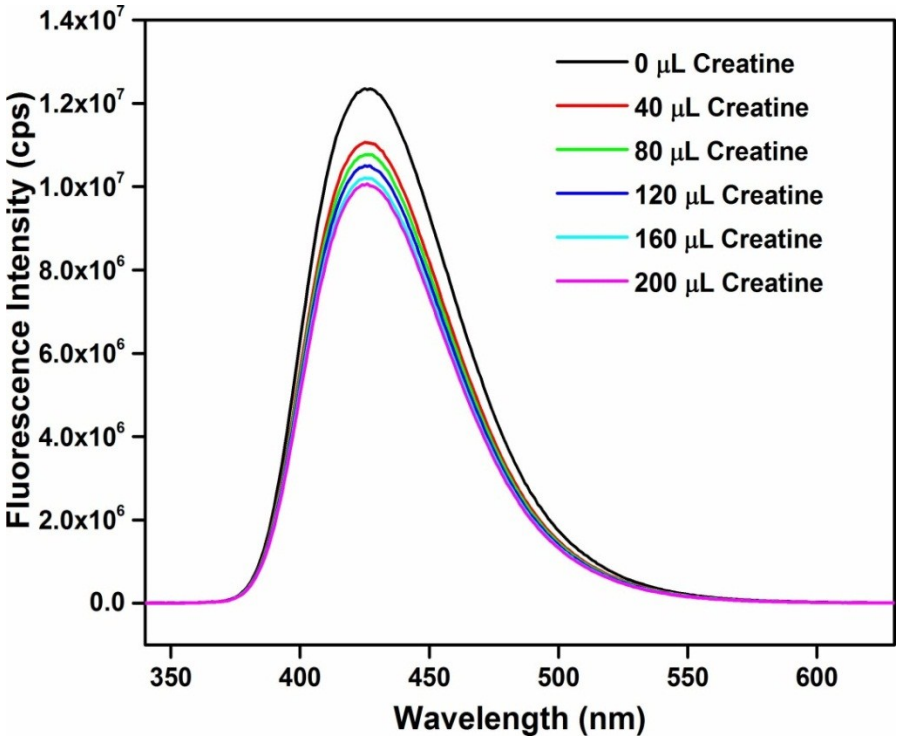

Figure S11. Change in the fluorescence emission intensity of **1-NH_2@THB** upon incremental addition of 1 mM creatine solution (λ_{ex}= 325 nm and λ_{em}= 429 nm).

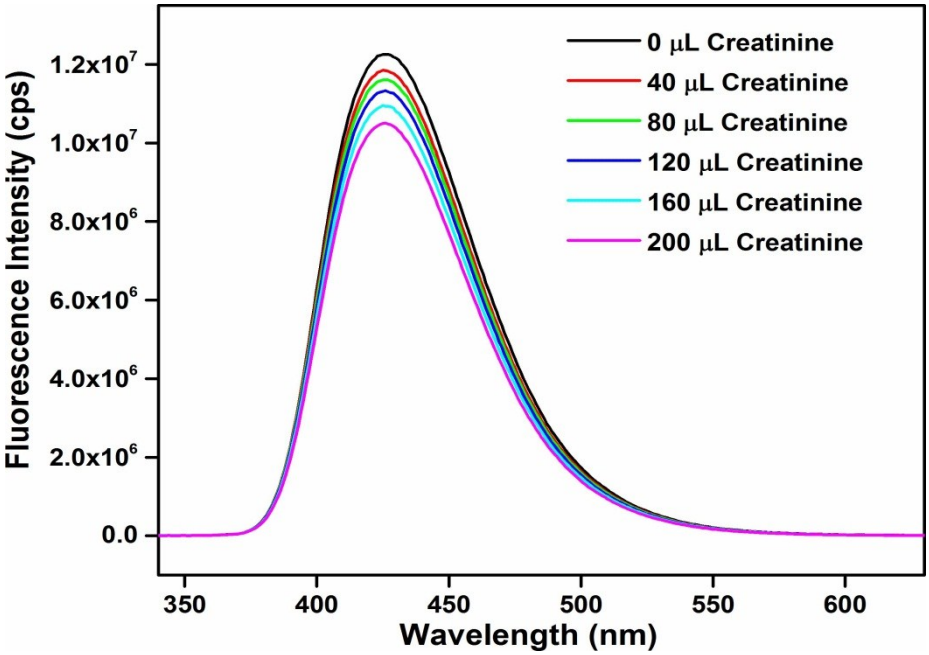

Figure S12. Change in the fluorescence emission intensity of **1-NH_2@THB** upon incremental addition of 1 mM creatinine solution (λ_{ex}= 325 nm and λ_{em}= 429 nm).

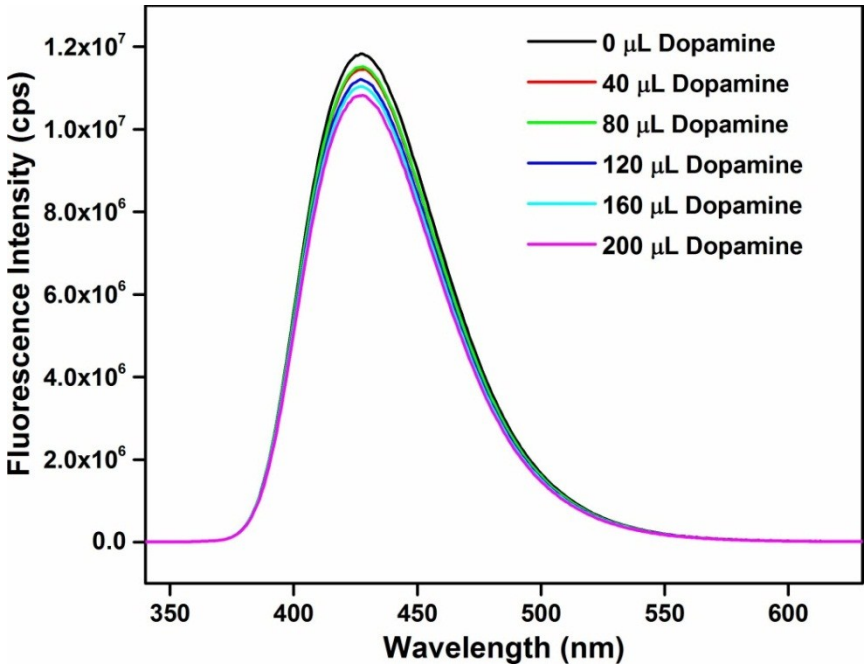

Figure S13. Change in the fluorescence emission intensity of **1-NH_2@THB** upon incremental addition of 1 mM dopamine solution (λ_{ex}= 325 nm and λ_{em}= 429 nm).

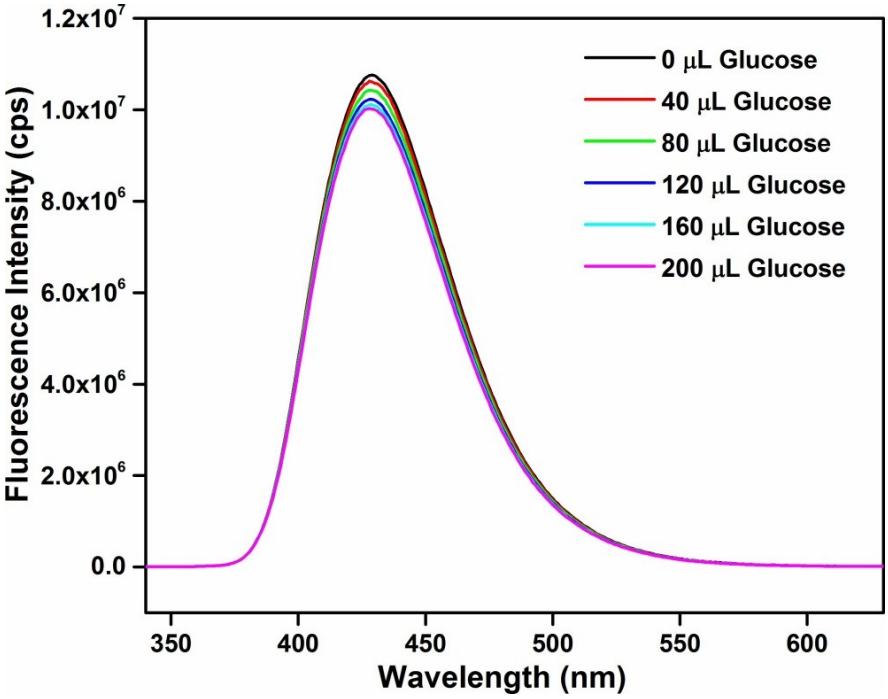

Figure S14. Change in the fluorescence emission intensity of **1-NH_2@THB** upon incremental addition of 1 mM glucose solution (λ_{ex}= 325 nm and λ_{em}= 429 nm).

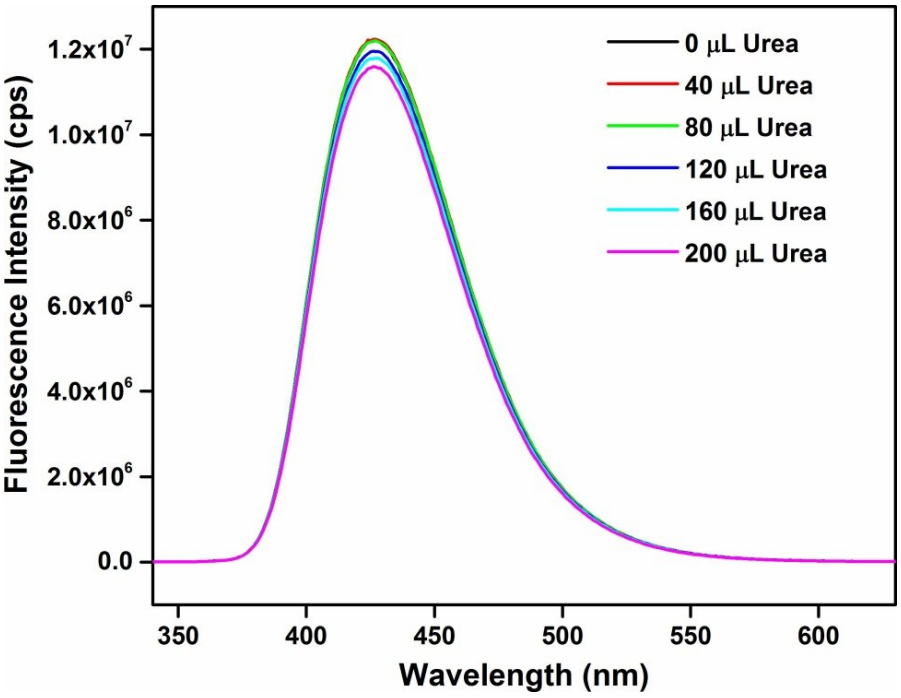

Figure S15. Change in the fluorescence emission intensity of **1-NH_2@THB** upon incremental addition of 1 mM urea solution (λ_{ex}= 325 nm and λ_{em}= 429 nm).

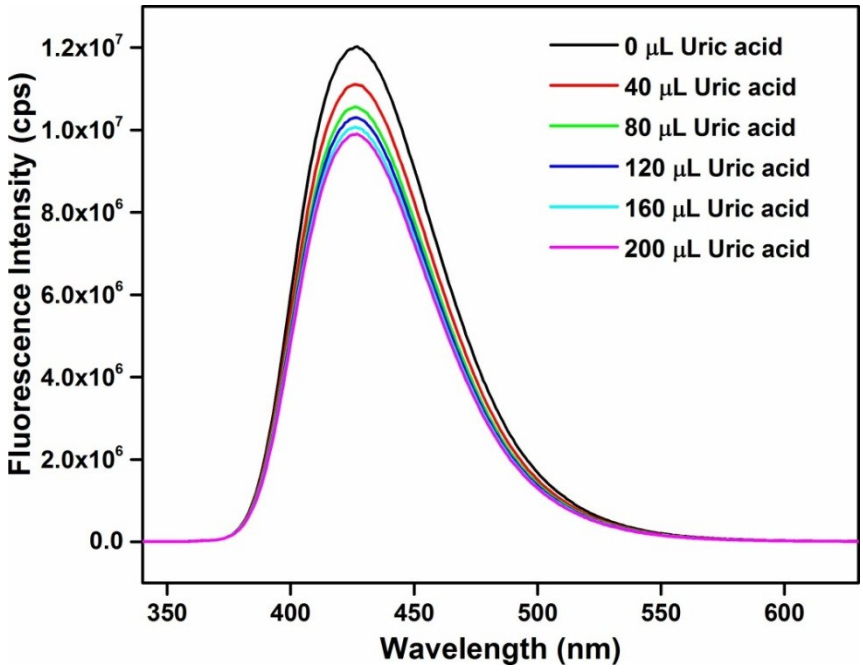

Figure S16. Change in the fluorescence emission intensity of **1-NH_2@THB** upon incremental addition of 1 mM uric acid solution (λ_{ex}= 325 nm and λ_{em}= 429 nm).

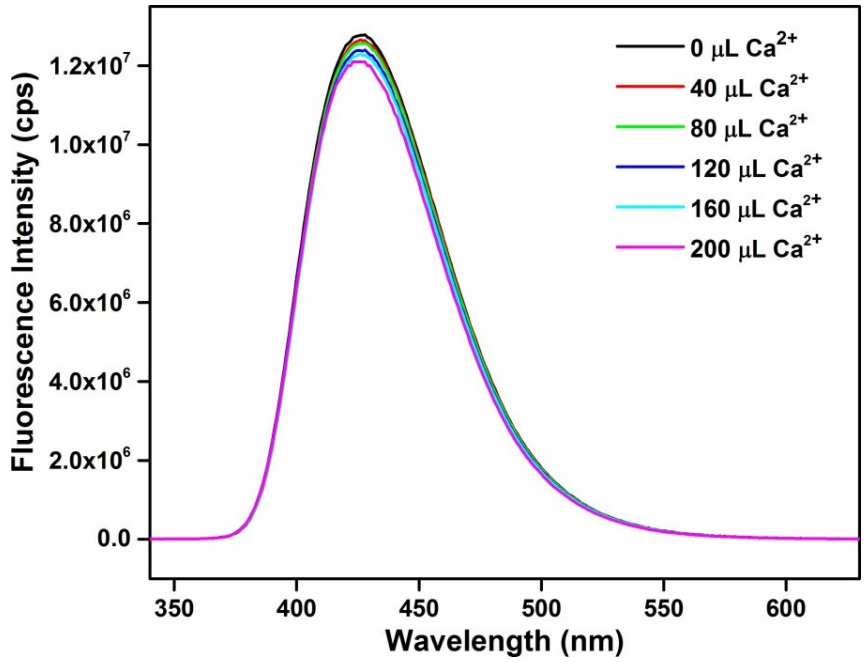

Figure S17. Change in the fluorescence emission intensity of **1-NH_2@THB** upon incremental addition of 1 mM Ca^{2+} solution (λ_{ex}= 325 nm and λ_{em}= 429 nm).

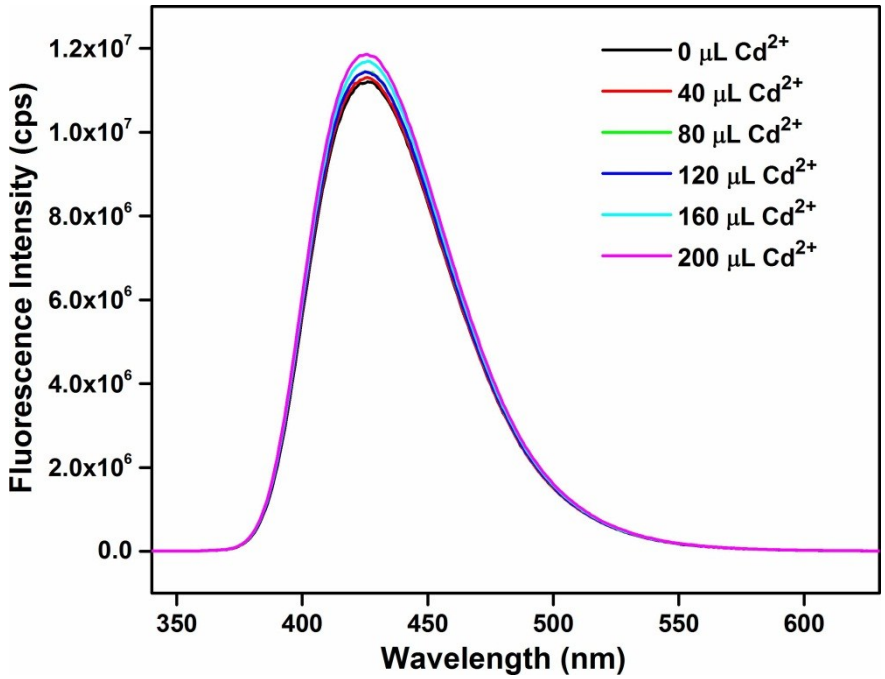

Figure S18. Change in the fluorescence emission intensity of **1-NH_2@THB** upon incremental addition of 1 mM Cd^{2+} solution (λ_{ex}= 325 nm and λ_{em}= 429 nm).

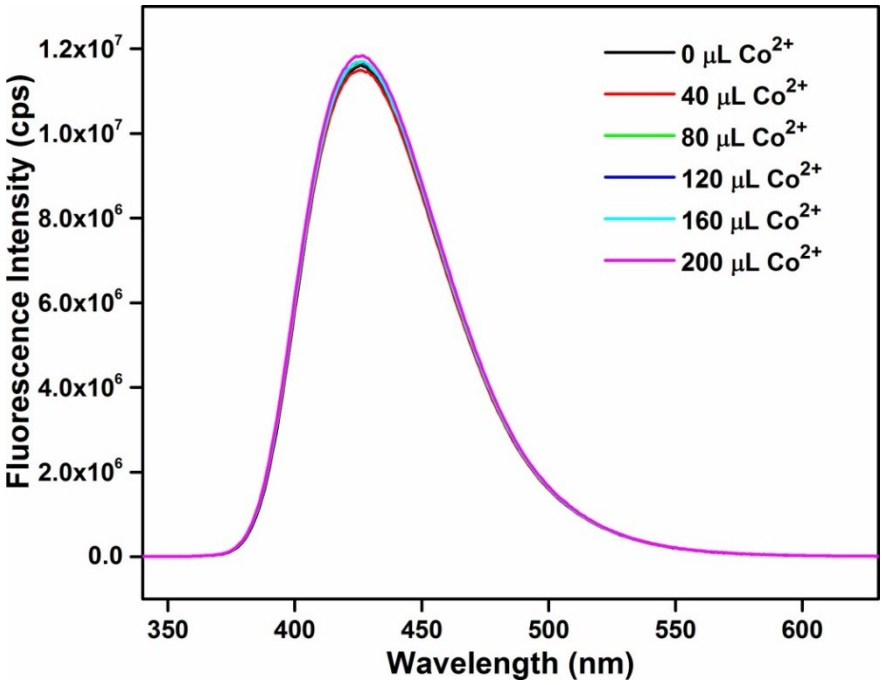

Figure S19. Change in the fluorescence emission intensity of **1-NH_2@THB** upon incremental addition of 1 mM Co^{2+} solution (λ_{ex}= 325 nm and λ_{em}= 429 nm).

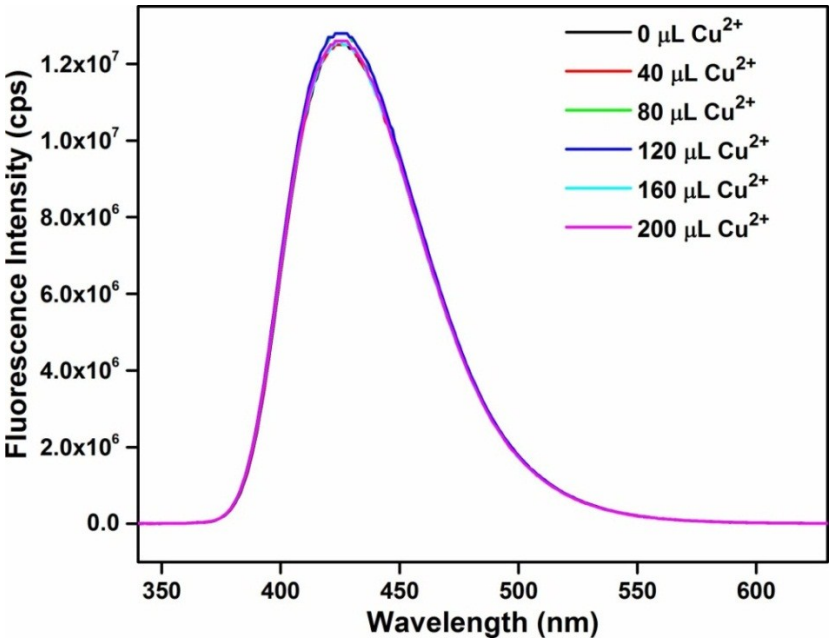

Figure S20. Change in the fluorescence emission intensity of **1-NH_2@THB** upon incremental addition of 1 mM Cu^{2+} solution (λ_{ex}= 325 nm and λ_{em}= 429 nm).

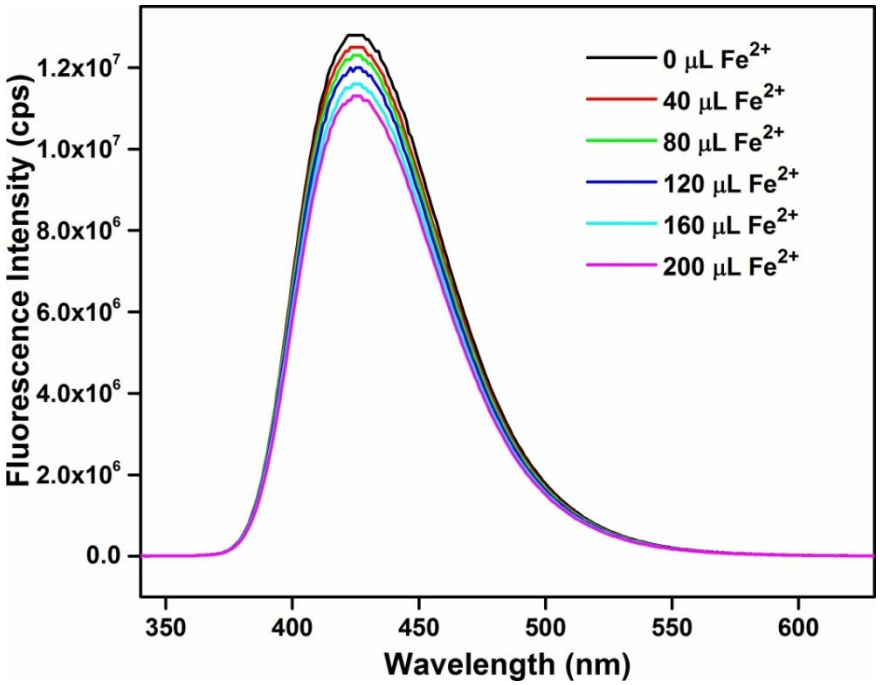

Figure S21. Change in the fluorescence emission intensity of **1-NH$_2$@THB** upon incremental addition of 1 mM Fe^{2+} solution (λ_{ex}= 325 nm and λ_{em}= 429 nm).

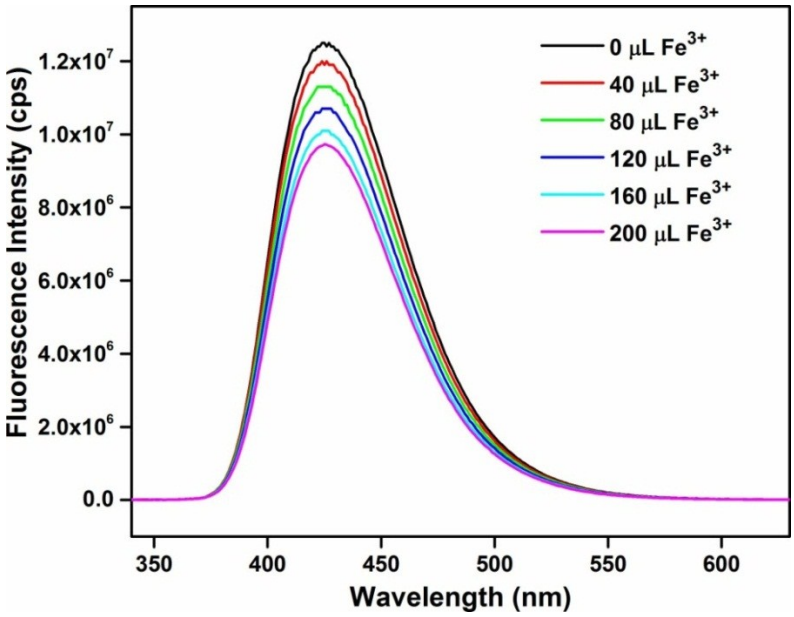

Figure S22. Change in the fluorescence emission intensity of **1-NH$_2$@THB** upon incremental addition of 1 mM Fe^{3+} solution (λ_{ex}= 325 nm and λ_{em}= 429 nm).

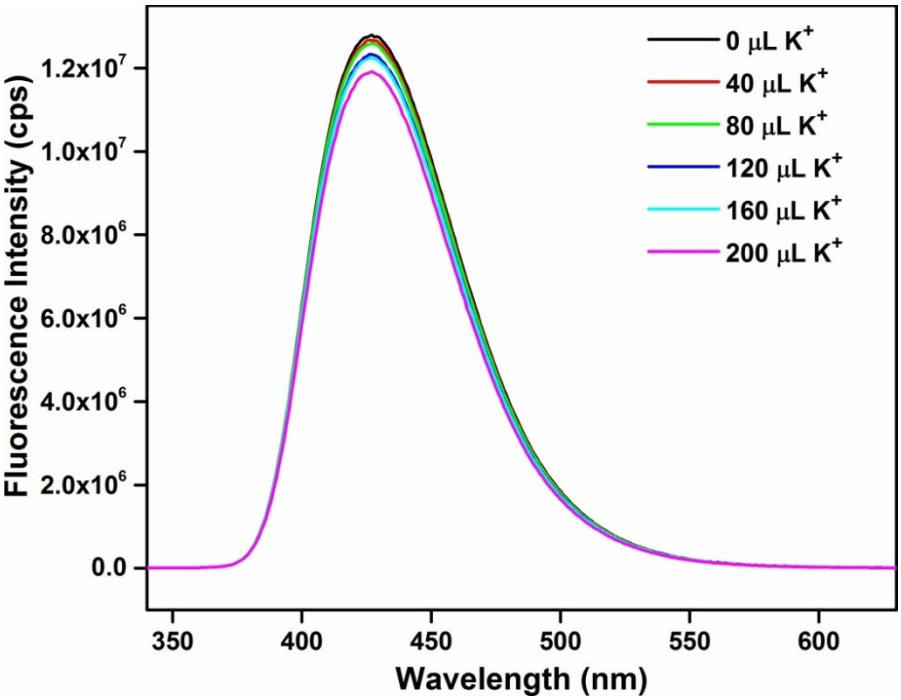

Figure S23. Change in the fluorescence emission intensity of **1-NH_2@THB** upon incremental addition of 1 mM K^+ solution (λ_{ex}= 325 nm and λ_{em}= 429 nm).

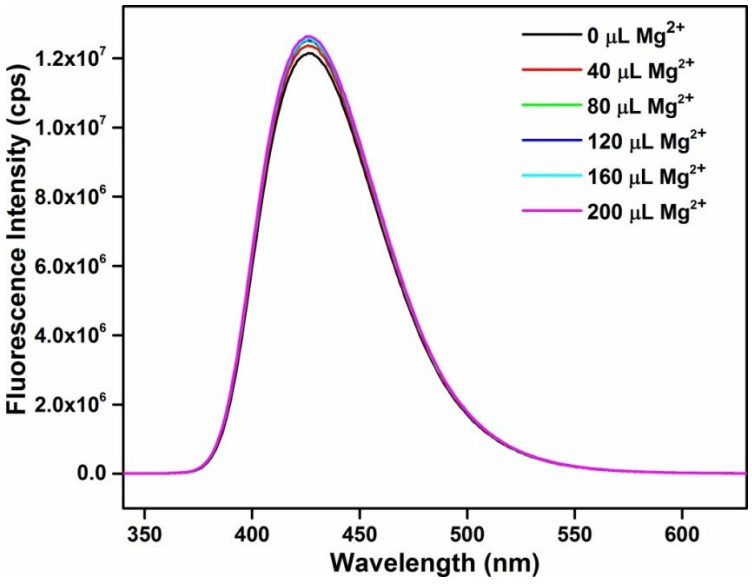

Figure S24. Change in the fluorescence emission intensity of **1-NH_2@THB** upon incremental addition of 1 mM Mg^{2+} solution (λ_{ex}= 325 nm and λ_{em}= 429 nm).

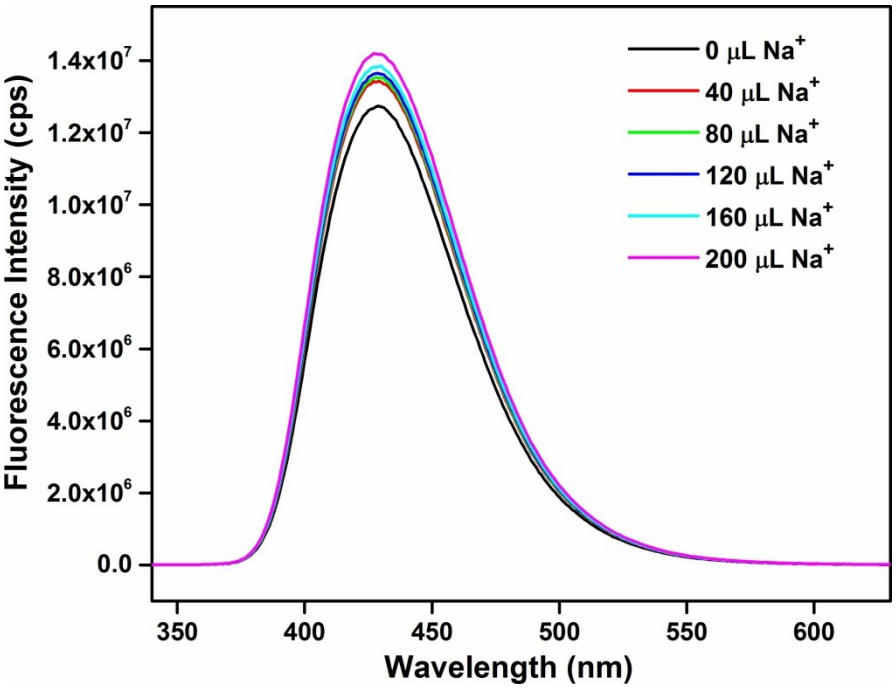

Figure S25. Change in the fluorescence emission intensity of **1-NH$_2$@THB** upon incremental addition of 1 mM Na^+ solution (λ_{ex}= 325 nm and λ_{em}= 429 nm).

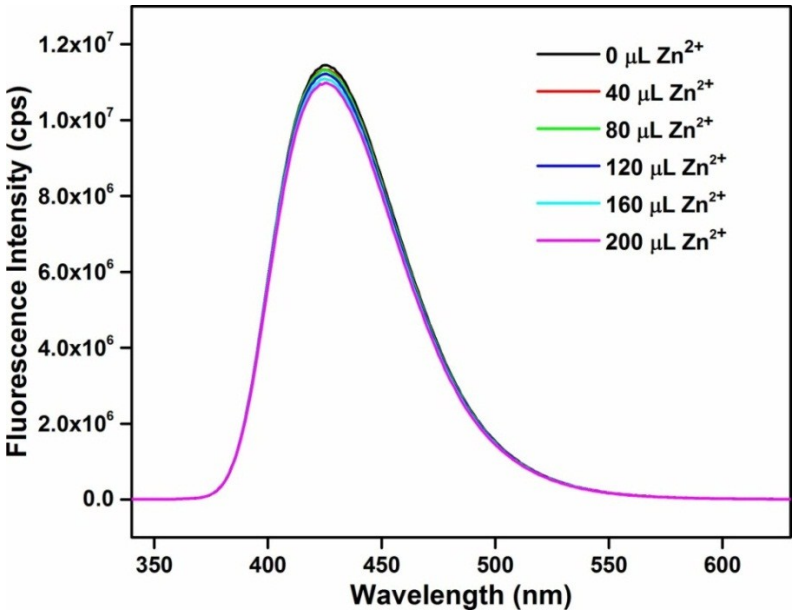

Figure S26. Change in the fluorescence emission intensity of **1-NH$_2$@THB** upon incremental addition of 1 mM Zn^{2+} solution (λ_{ex}= 325 nm and λ_{em}= 429 nm).

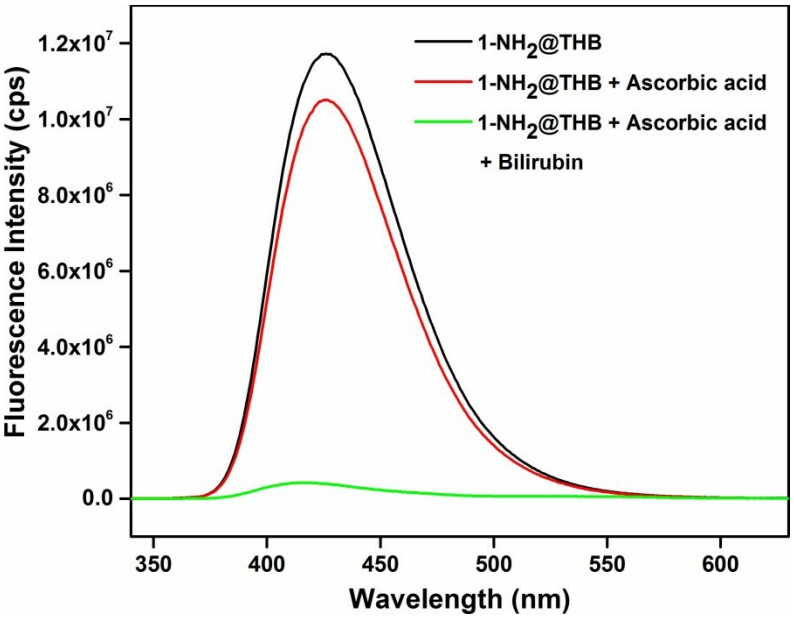

Figure S27. Change in the fluorescence emission intensity of **1-NH_2@THB** upon addition of 1 mM bilirubin solution (200 µL) in presence of ascorbic acid (200 µL) solution (λ_{ex}= 325 nm and λ_{em}= 429 nm).

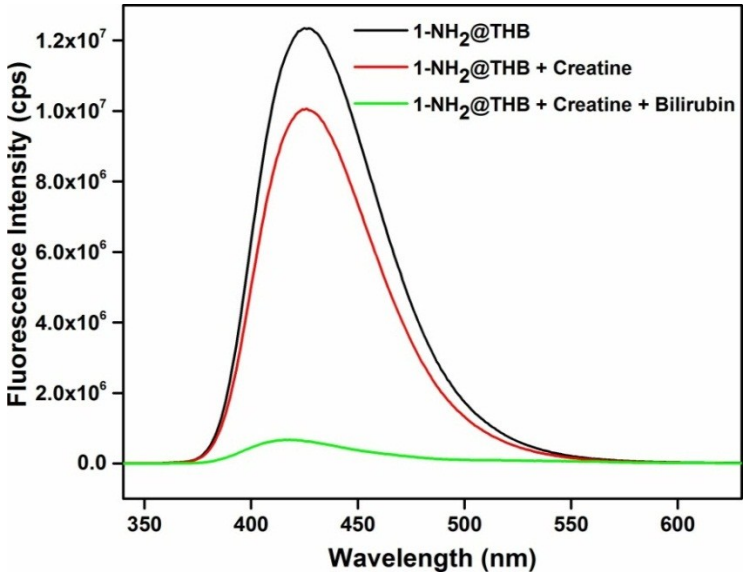

Figure S28. Change in the fluorescence emission intensity of **1-NH_2@THB** upon addition of 1 mM bilirubin solution (200 µL) in presence of creatine (200 µL) solution (λ_{ex}= 325 nm and λ_{em}= 429 nm).

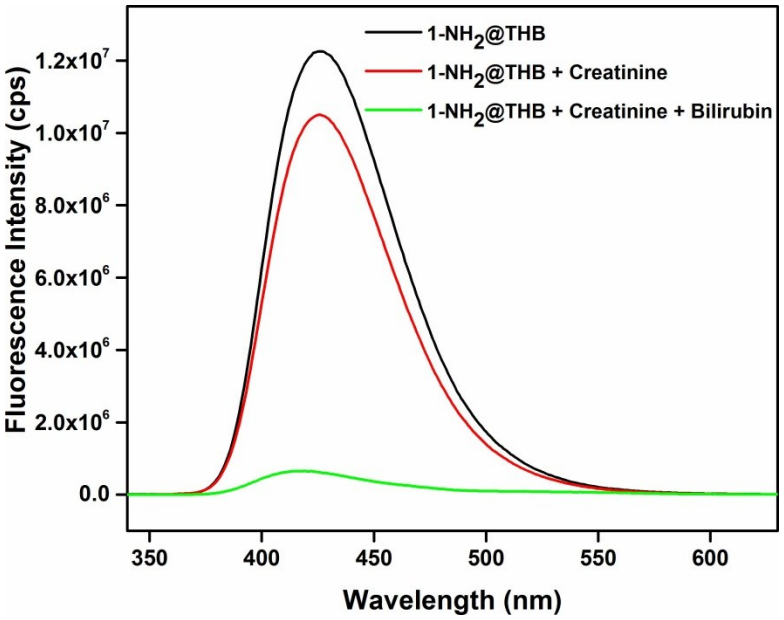

Figure S29. Change in the fluorescence emission intensity of **1-NH_2@THB** upon addition of 1 mM bilirubin solution (200 µL) in presence of creatinine (200 µL) solution (λ_{ex}= 325 nm and λ_{em}= 429 nm).

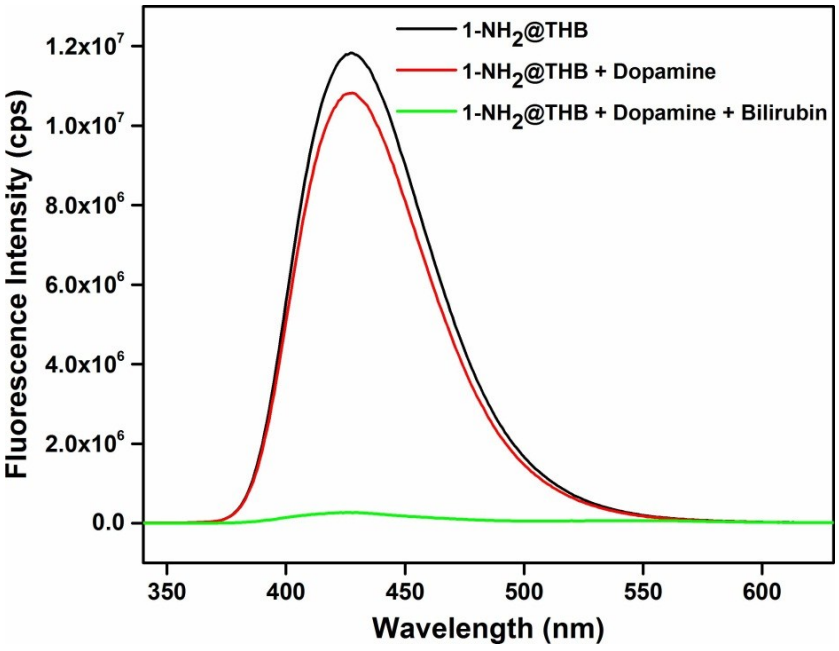

Figure S30. Change in the fluorescence emission intensity of **1-NH_2@THB** upon addition of 1 mM bilirubin solution (200 µL) in presence of dopamine (200 µL) solution (λ_{ex}= 325 nm and λ_{em}= 429 nm).

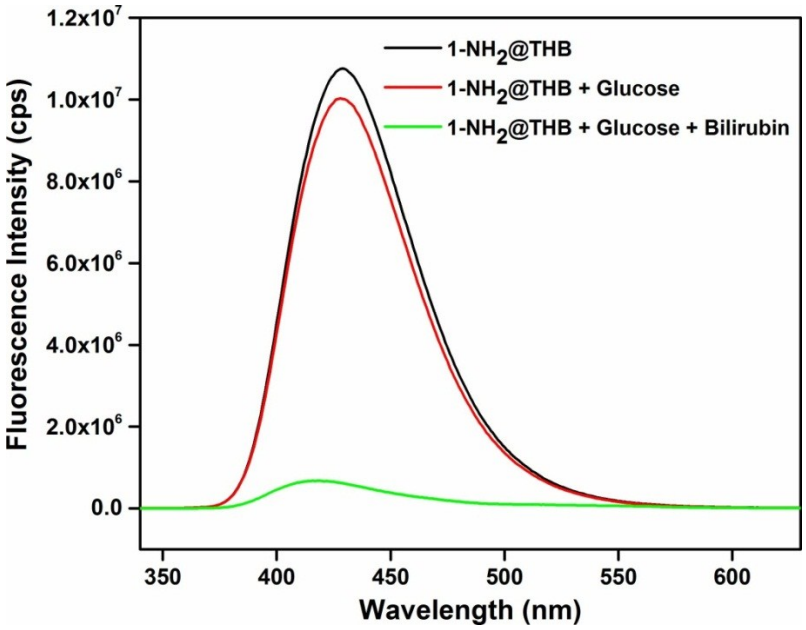

Figure S31. Change in the fluorescence emission intensity of **1-NH_2@THB** upon addition of 1 mM bilirubin solution (200 µL) in presence of glucose (200 µL) solution (λ_{ex}= 325 nm and λ_{em}= 429 nm).

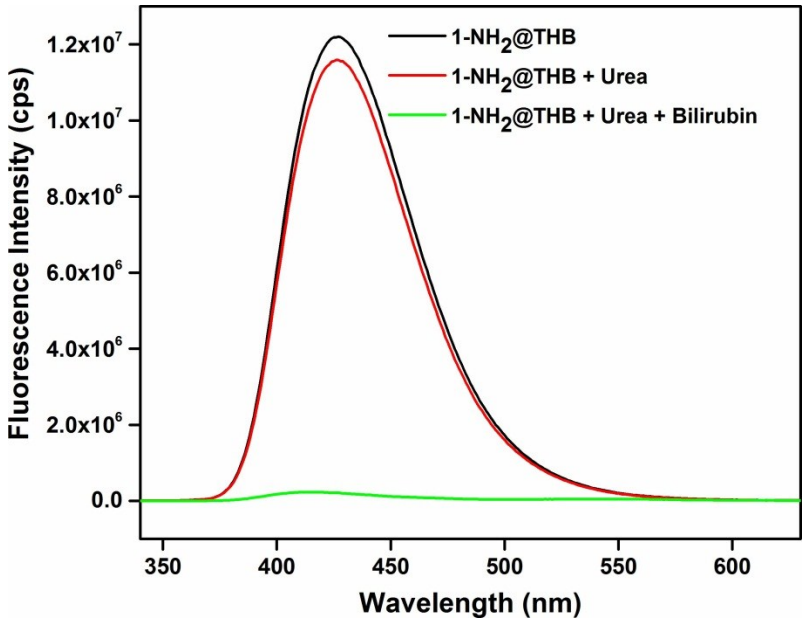

Figure S32. Change in the fluorescence emission intensity of **1-NH_2@THB** upon addition of 1 mM bilirubin solution (200 µL) in presence of urea (200 µL) solution (λ_{ex}= 325 nm and λ_{em}= 429 nm).

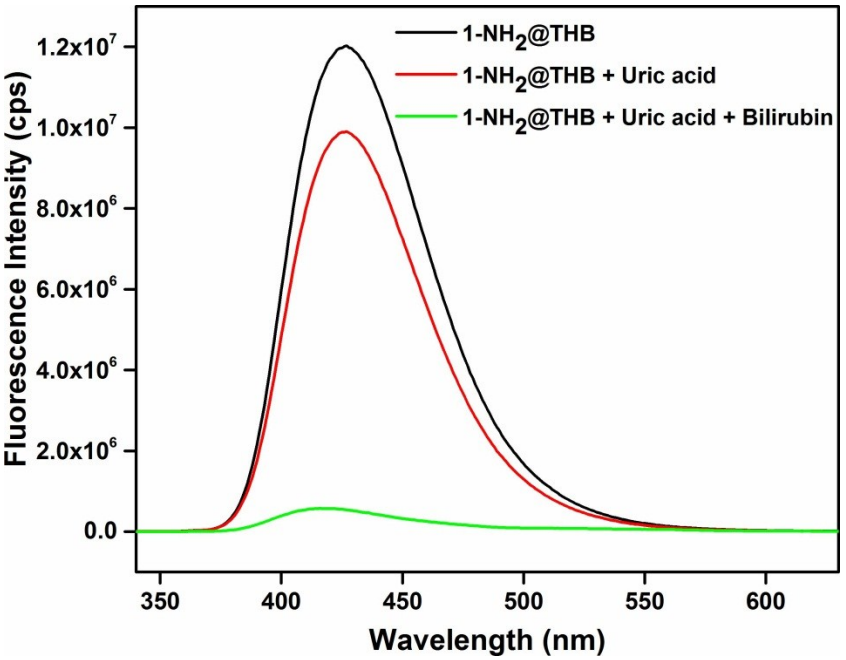

Figure S33. Change in the fluorescence emission intensity of **1-NH_2@THB** upon addition of 1 mM bilirubin solution (200 µL) in presence of uric acid (200 µL) solution (λ_{ex}= 325 nm and λ_{em}= 429 nm).

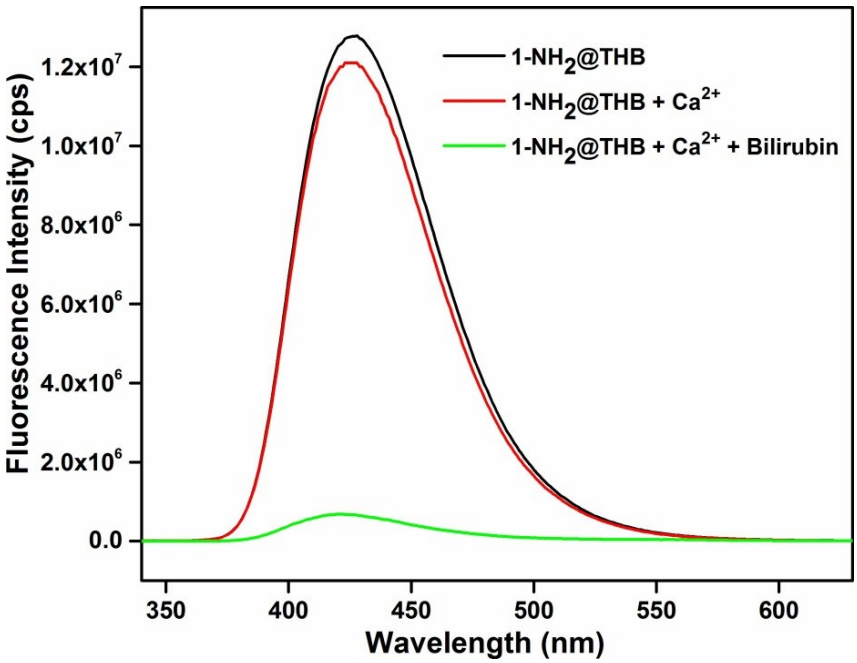

Figure S34. Change in the fluorescence emission intensity of **1-NH_2@THB** upon addition of 1 mM bilirubin solution (200 µL) in presence of Ca^{2+} (200 µL) solution (λ_{ex}= 325 nm and λ_{em}= 429 nm).

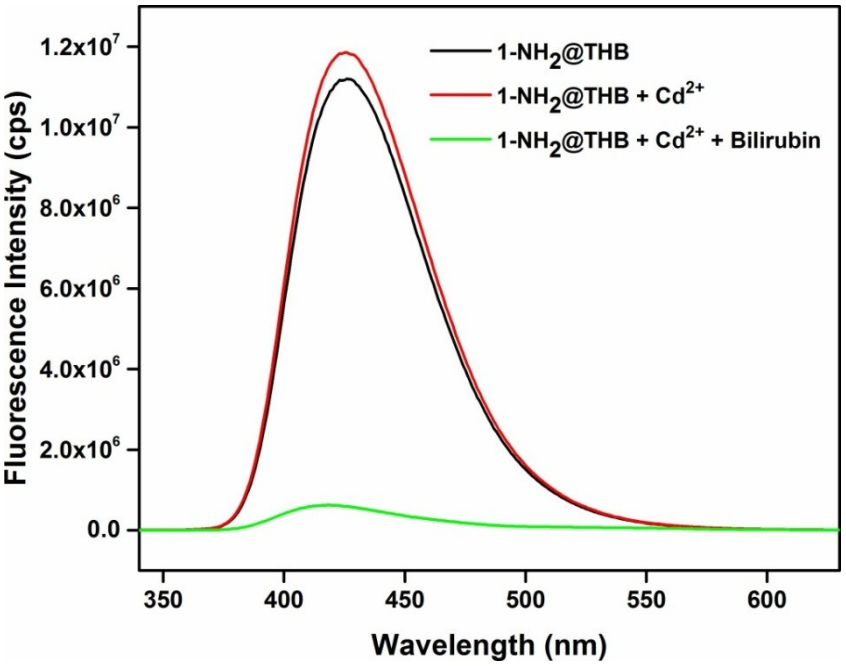

Figure S35. Change in the fluorescence emission intensity of **1-NH_2@THB** upon addition of 1 mM bilirubin solution (200 µL) in presence of Cd^{2+} (200 µL) solution (λ_{ex}= 325 nm and λ_{em}= 429 nm).

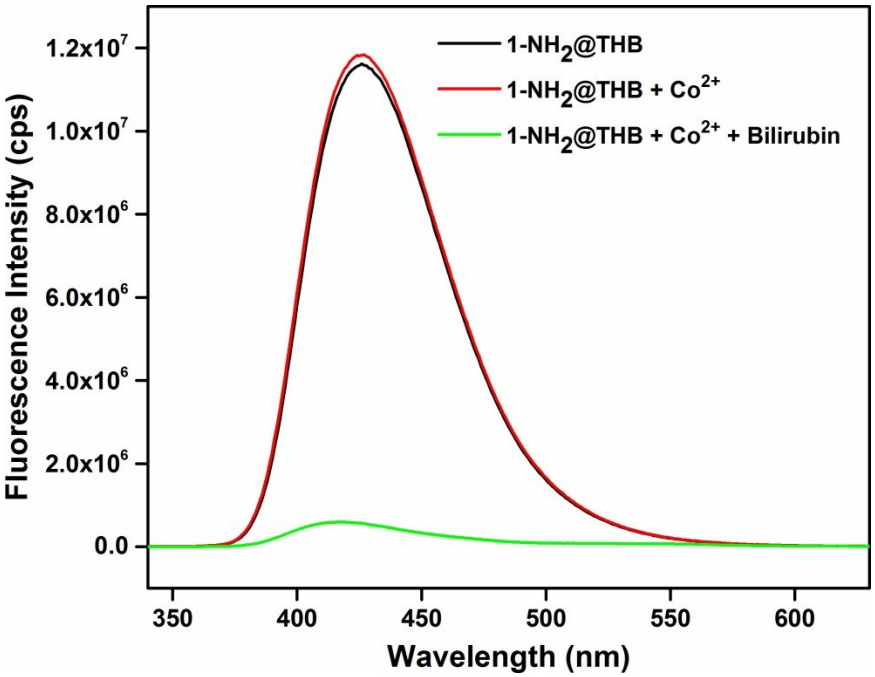

Figure S36. Change in the fluorescence emission intensity of **1-NH_2@THB** upon addition of 1 mM bilirubin solution (200 µL) in presence of Co^{2+} (200 µL) solution (λ_{ex}= 325 nm and λ_{em}= 429 nm).

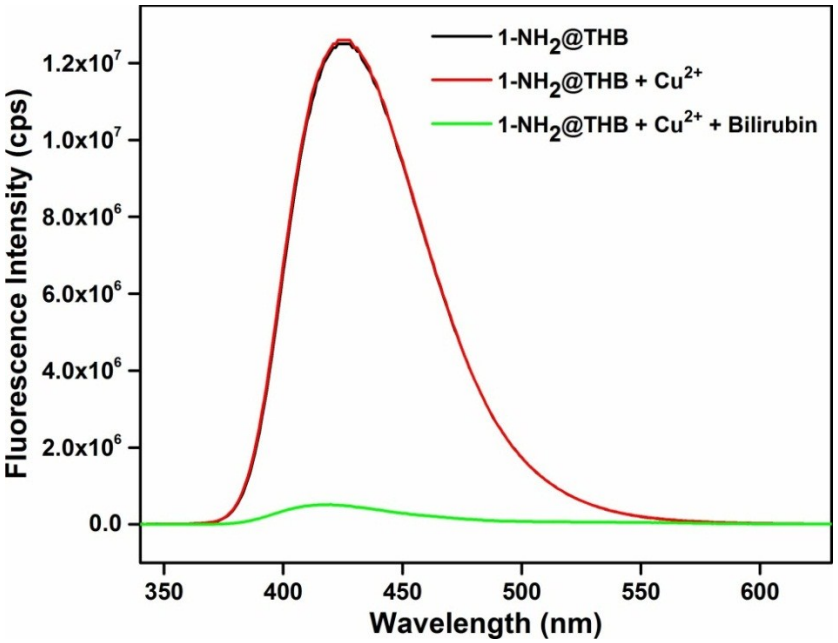

Figure S37. Change in the fluorescence emission intensity of **1-NH_2@THB** upon addition of 1 mM bilirubin solution (200 µL) in presence of Cu^{2+} (200 µL) solution (λ_{ex}= 325 nm and λ_{em}= 429 nm).

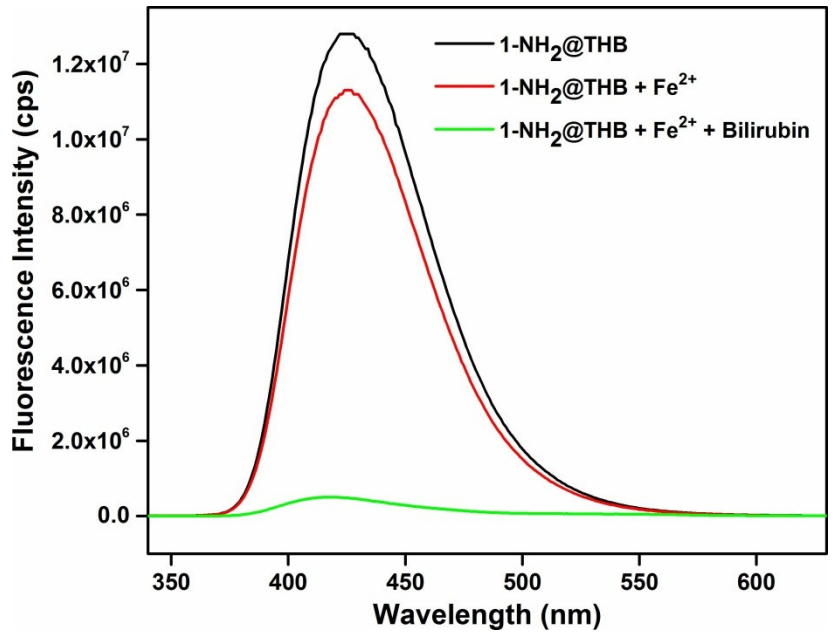

Figure S38. Change in the fluorescence emission intensity of **1-NH_2@THB** upon addition of 1 mM bilirubin solution (200 µL) in presence of Fe^{2+} (200 µL) solution (λ_{ex}= 325 nm and λ_{em}= 429 nm).

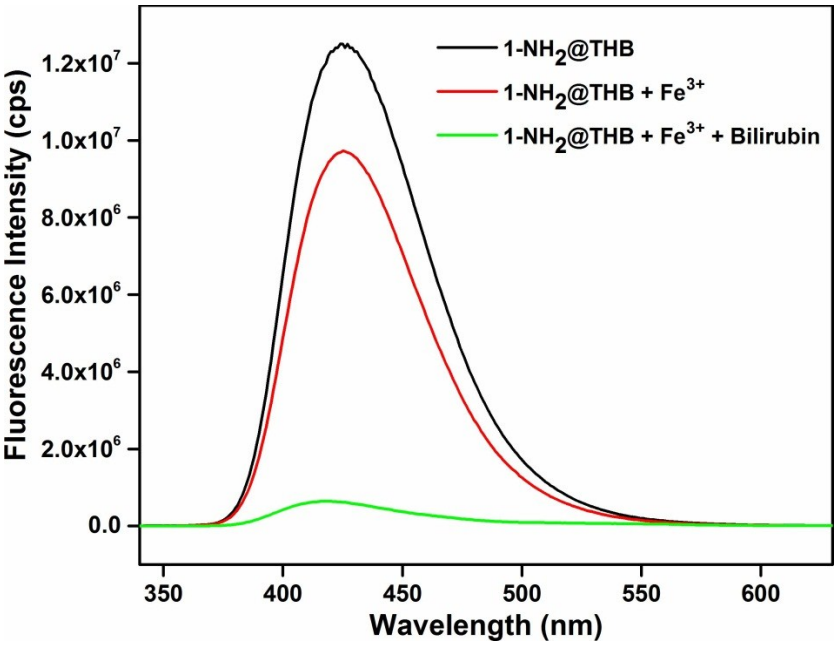

Figure S39. Change in the fluorescence emission intensity of **1-NH_2@THB** upon addition of 1 mM bilirubin solution (200 µL) in presence of Fe^{3+} (200 µL) solution (λ_{ex}= 325 nm and λ_{em}= 429 nm).

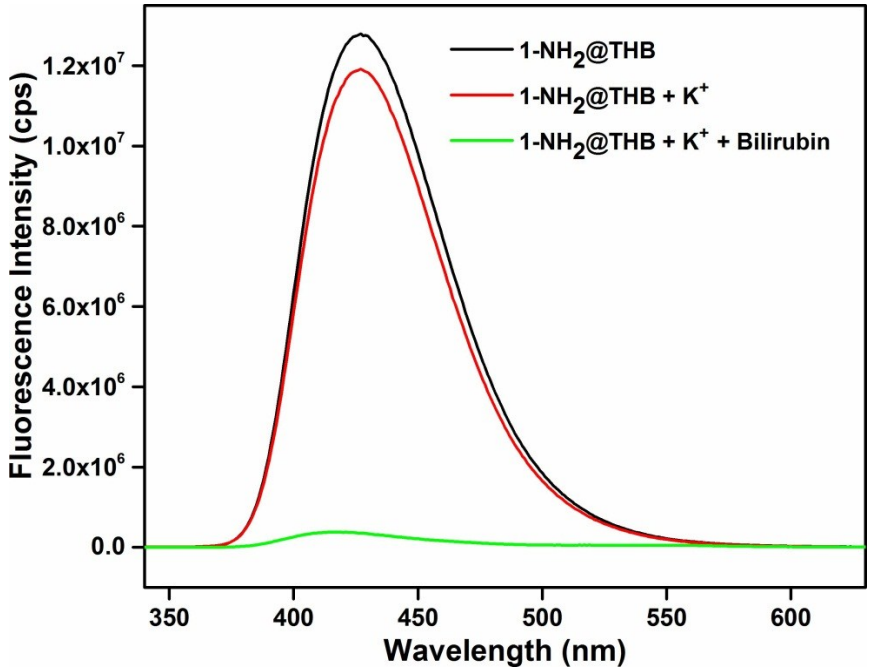

Figure S40. Change in the fluorescence emission intensity of **1-NH_2@THB** upon addition of 1 mM bilirubin solution (200 µL) in presence of K^+ (200 µL) solution (λ_{ex}= 325 nm and λ_{em}= 429 nm).

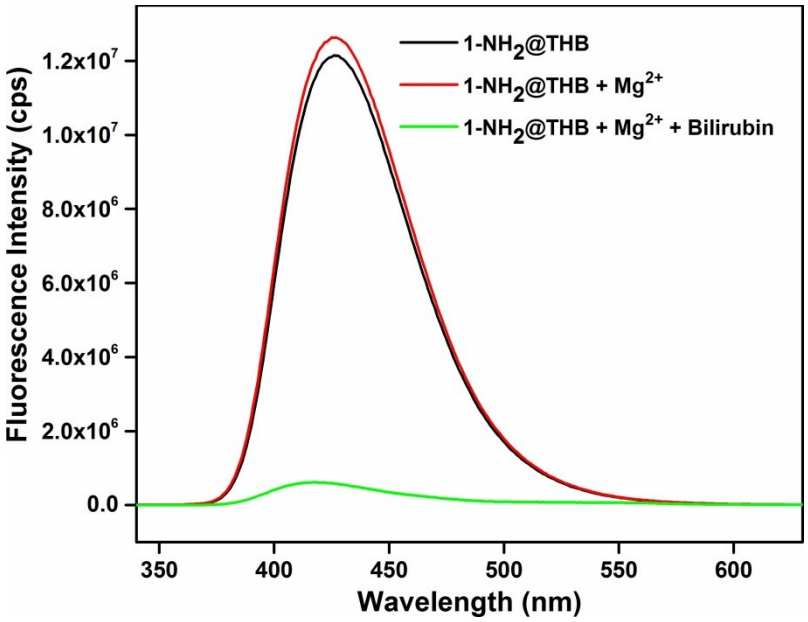

Figure S41. Change in the fluorescence emission intensity of **1-NH_2@THB** upon addition of 1 mM bilirubin solution (200 µL) in presence of Mg^{2+} (200 µL) solution (λ_{ex}= 325 nm and λ_{em}= 429 nm).

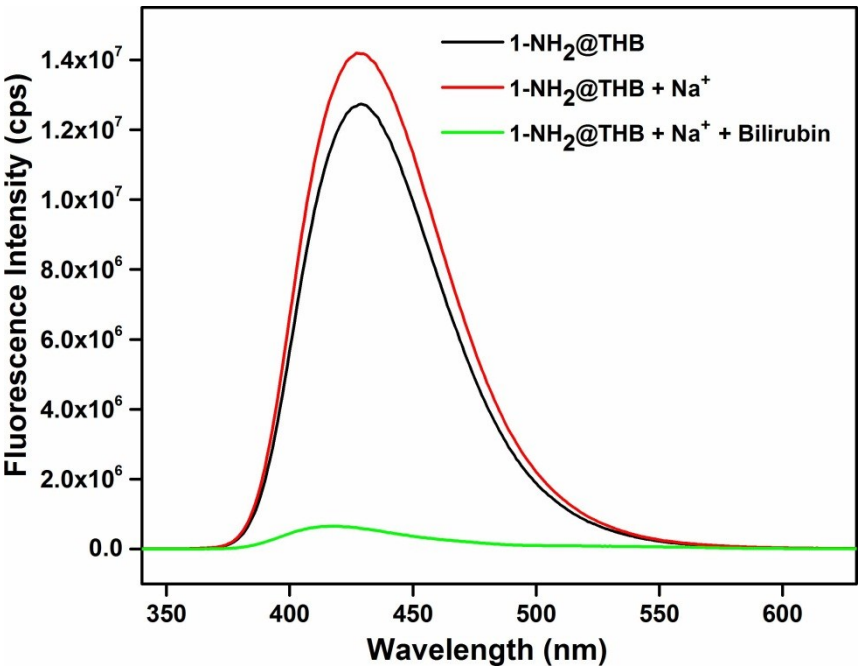

Figure S42. Change in the fluorescence emission intensity of **1-NH_2@THB** upon addition of 1 mM bilirubin solution (200 µL) in presence of Na^{+} (200 µL) solution (λ_{ex}= 325 nm and λ_{em}= 429 nm).

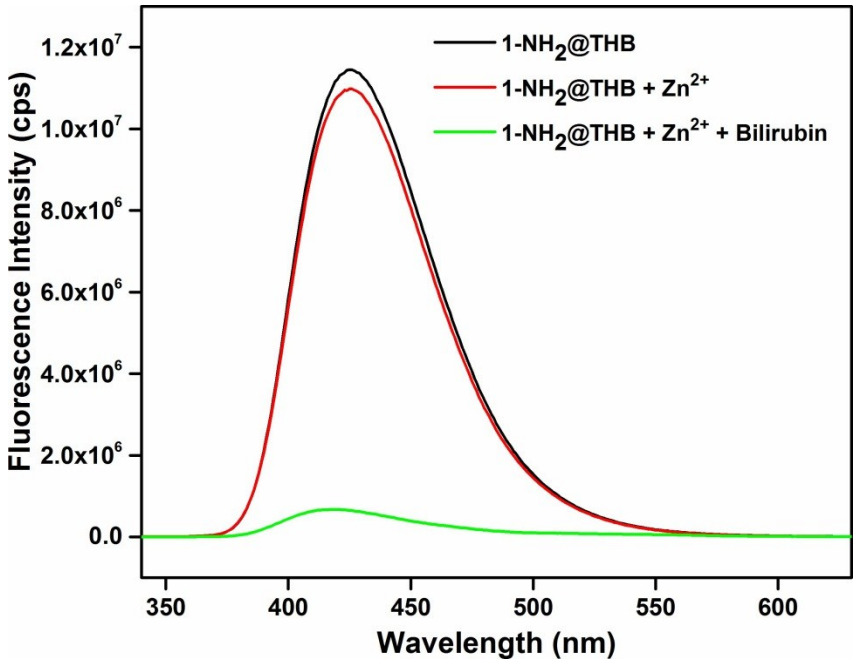

Figure S43. Change in the fluorescence emission intensity of **1-NH_2@THB** upon addition of 1 mM bilirubin solution (200 µL) in presence of Zn^{2+} (200 µL) solution (λ_{ex}= 325 nm and λ_{em}= 429 nm).

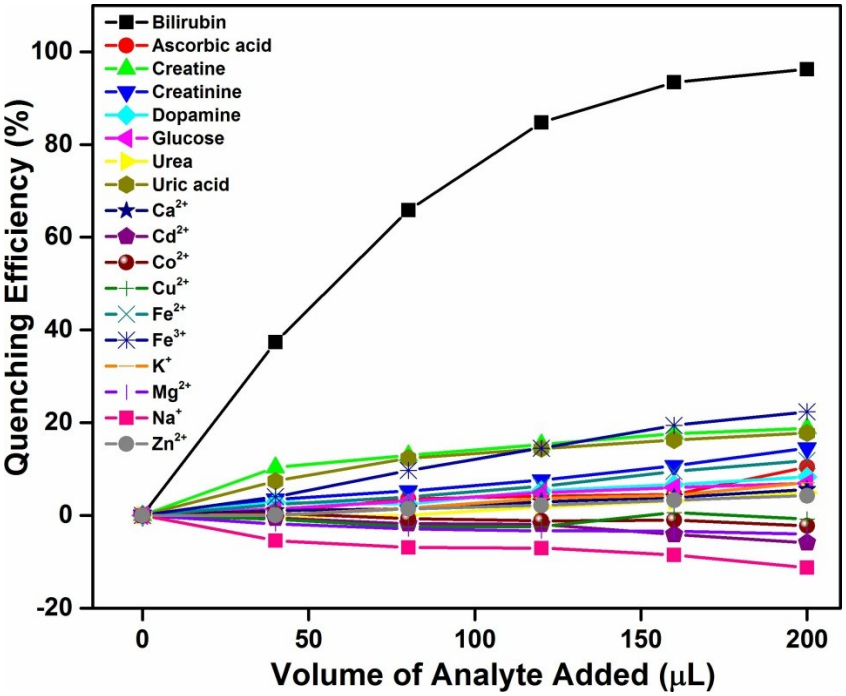

Figure S44. Variation of the fluorescence quenching efficiencies upon incremental addition of 1 mM solution of different competitive analytes to a 3 mL suspension of **1-NH_2@THB.**

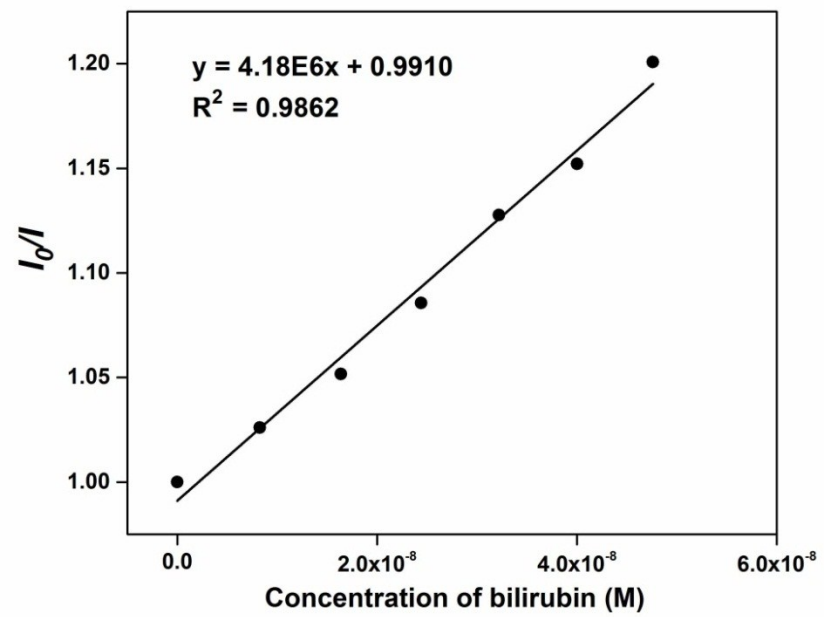

Figure S45. Stern-Volmer plot for the fluorescence emission quenching of **1-NH_2@THB** in presence of bilirubin solution.

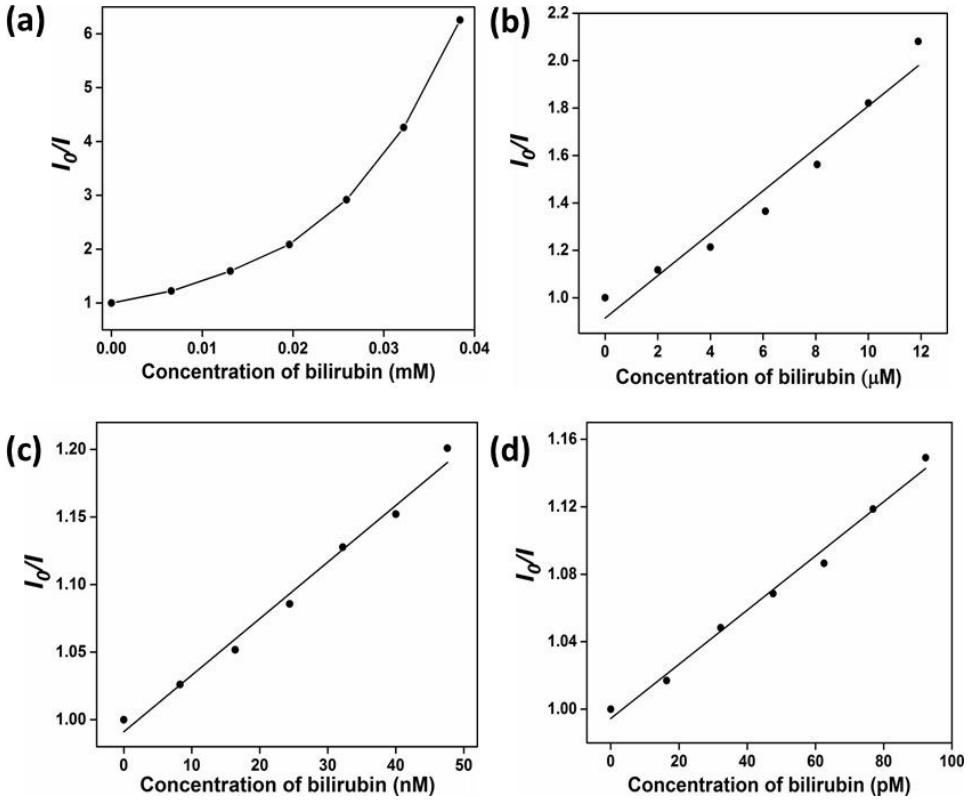

Figure S46. Relationships between I_0/I and concentrations of bilirubin in mili- (a), micro- (b), nano- (c), and picomolar (d) levels.

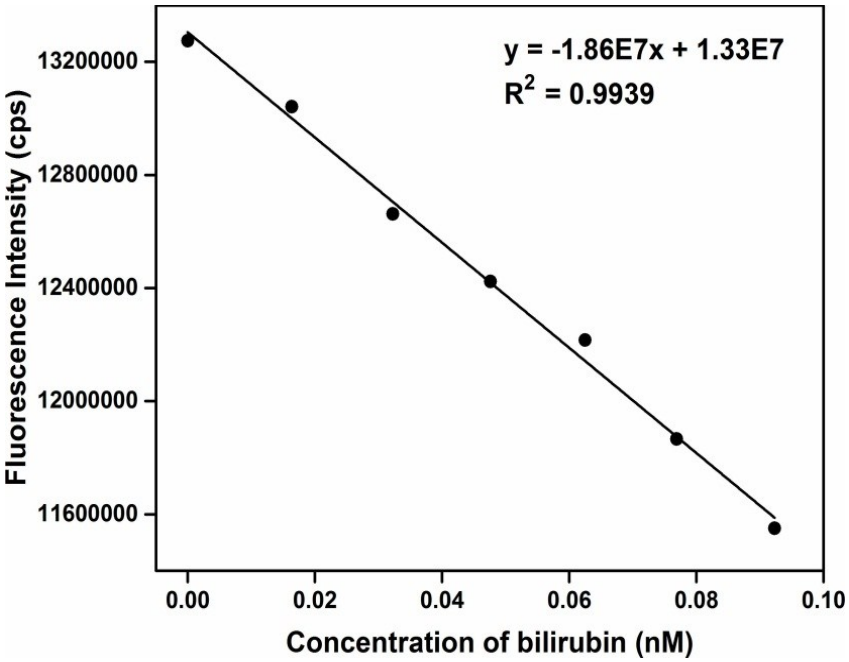

Figure S47. Change in the fluorescence emission intensity of **1-NH_2@THB** in HEPES buffer as a function of bilirubin concentration.

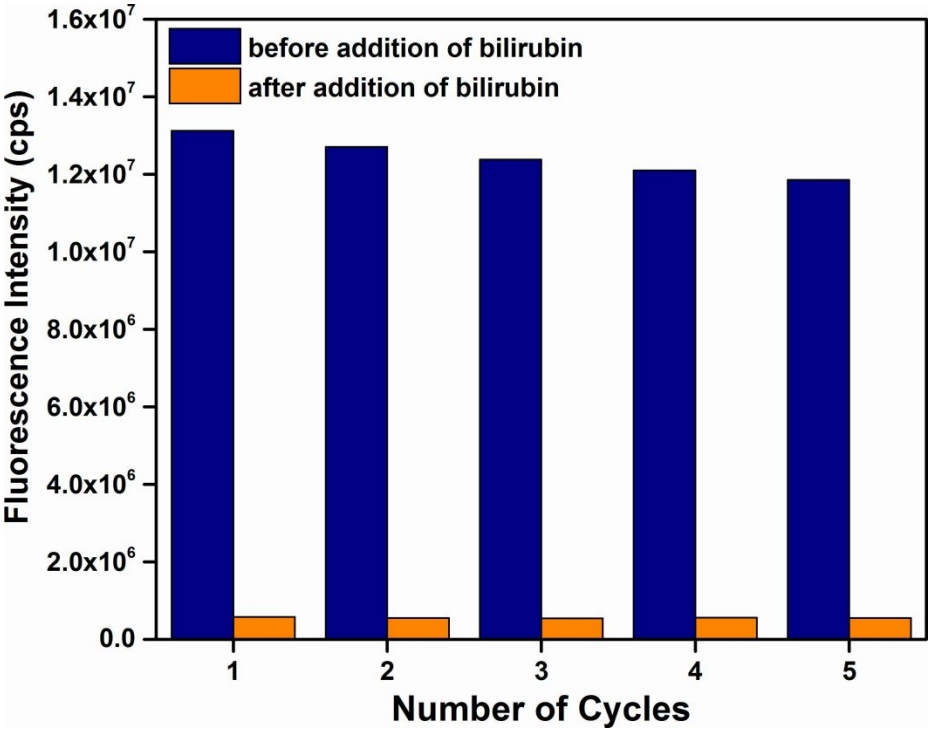

Figure S48. Recyclability of the quenching efficiency of the HEPES buffer suspension of **1-NH_2@THB** towards 1 mM bilirubin solution.

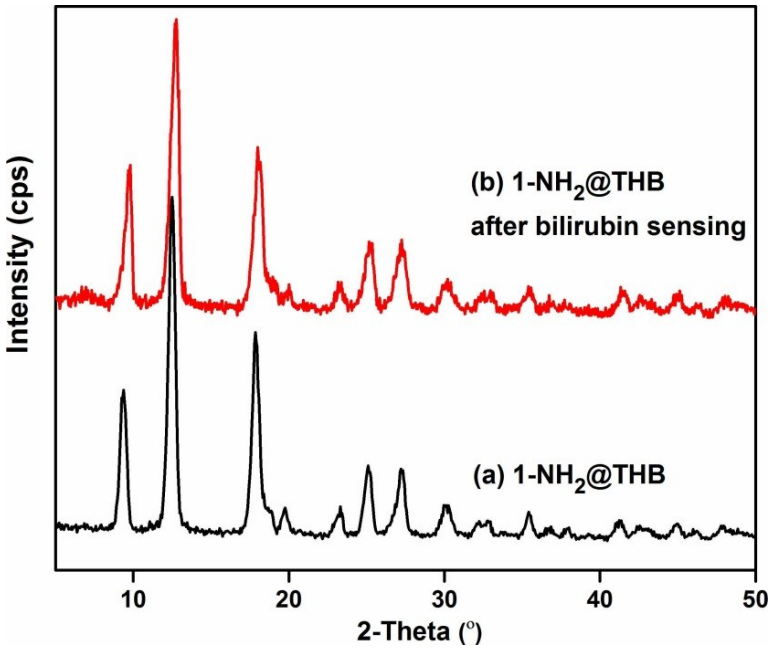

Figure S49. XRPD patterns of **1-NH_2@THB** before (a) and after sensing of bilirubin (b).

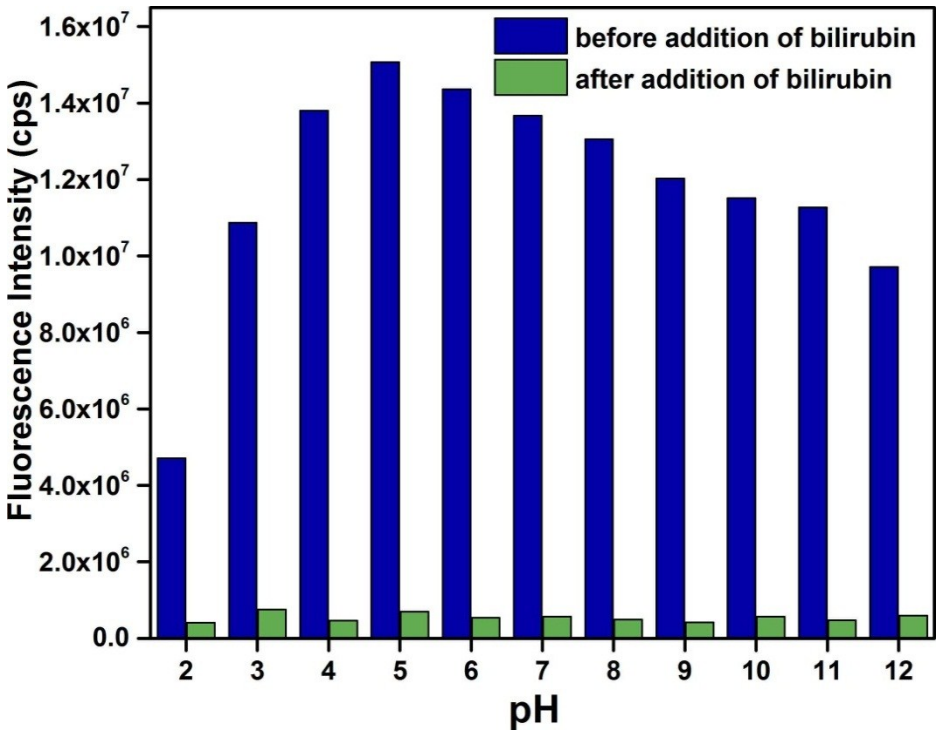

Figure S50. Effect of pH on fluorescence emission intensity of **1-NH_2@THB** before and after addition of 1 mM bilirubin solution (200 μL).

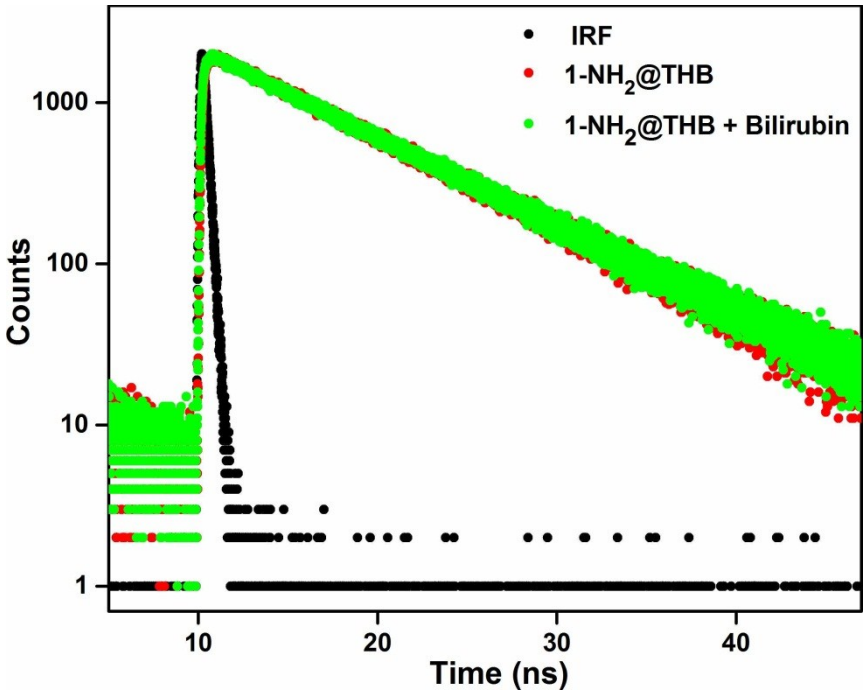

Figure S51. Lifetime decay profile of **1-NH_2@THB** in the absence and presence of bilirubin solution (λ_{ex} = 336 nm, monitored at 429 nm).

Table S1. Fluorescence lifetimes of **1-NH_2@THB** before and after the addition of bilirubin ((λ_{ex} = 336 nm, pulsed diode laser).

Volume of bilirubin (μL)	a_1	a_2	τ_1 (ns)	τ_2 (ns)	$\langle\tau\rangle^*$ (ns)	χ^2
0	0.985	0.014	7.852	0.019	7.734	1.012
200	0.990	0.009	7.675	0.028	7.598	1.013

Average lifetime $\langle\tau\rangle^* = a_1 \tau_1 + a_2 \tau_2$

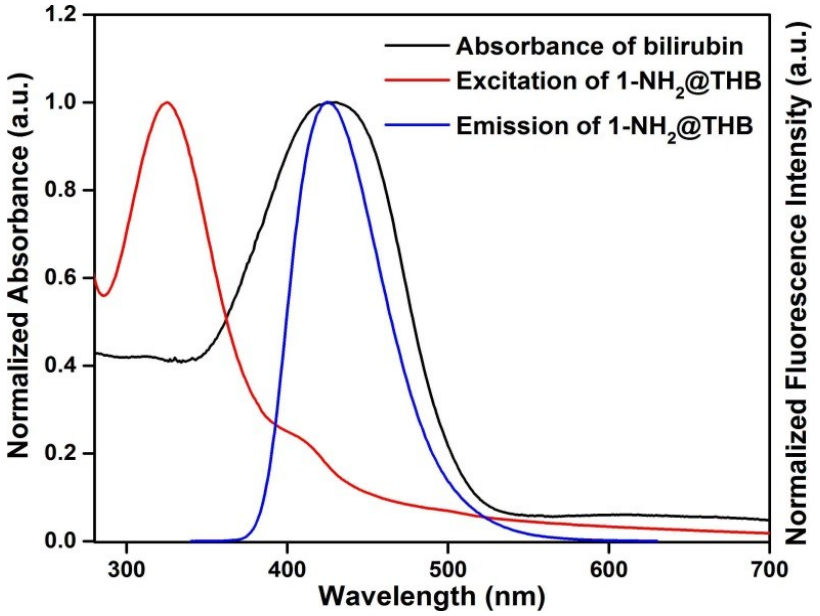

Figure S52. Normalized UV−vis spectrum of bilirubin overlapped with the normalized emission/excitation spectra of **1-NH_2@THB** in HEPES buffer.

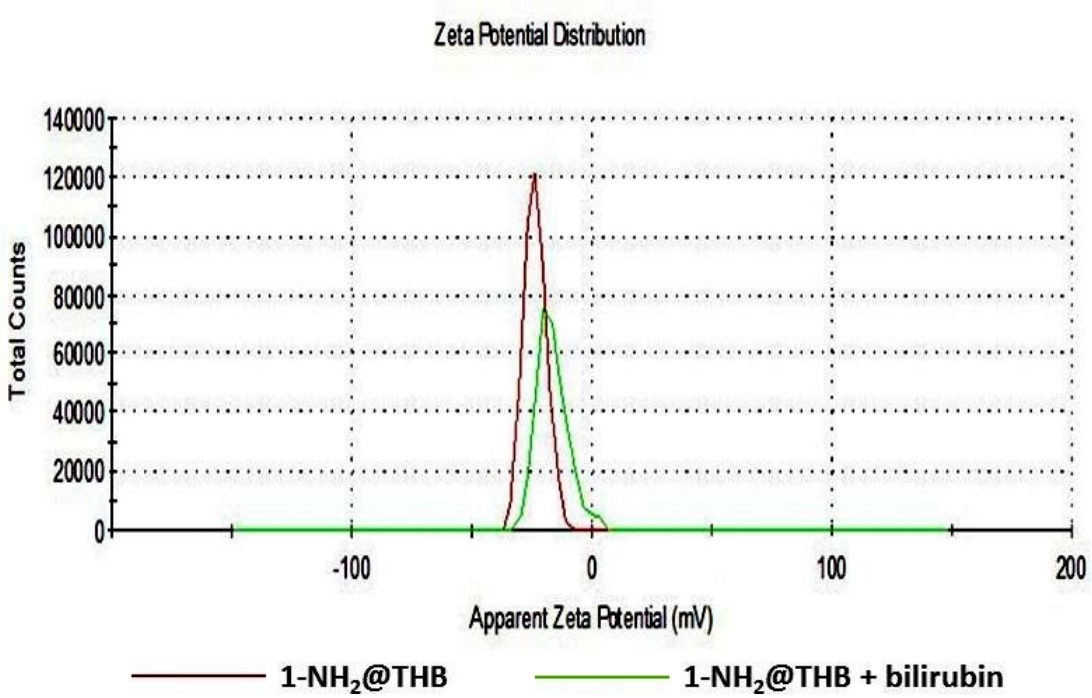

Figure S53. Zeta potential distribution of **1-NH_2@THB** in HEPES buffer medium (pH = 7.4) before and after addition of bilirubin.

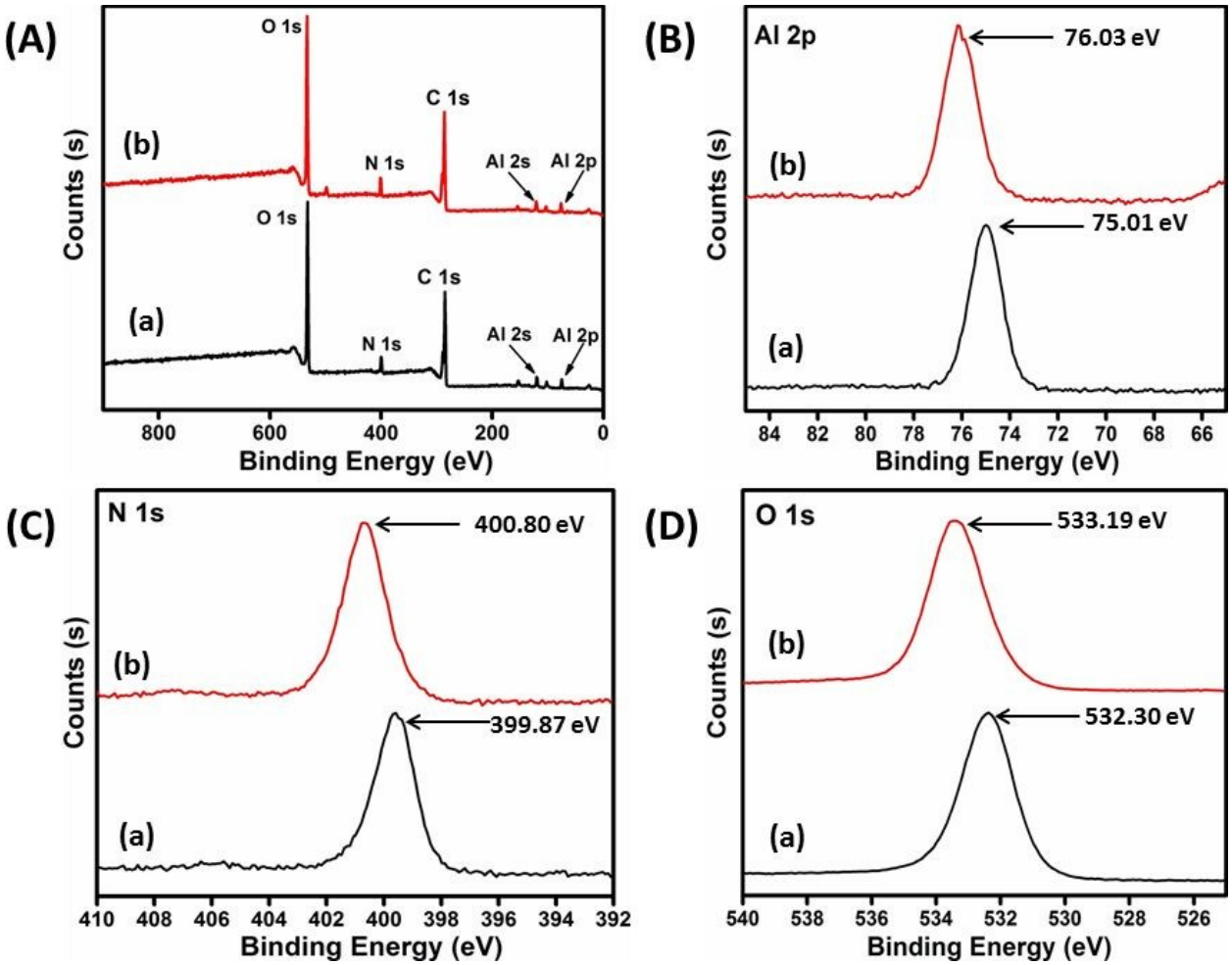

Figure S54. (A) XPS spectra of **1-NH_2@THB** (a) and bilirubin-treated **1-NH_2@THB** (b). High resolution XPS spectra of (B) Al 2p, (C) N 1s and (D) O 1s of **1-NH_2@THB** (a) and bilirubin-treated **1-NH_2@THB** (b).

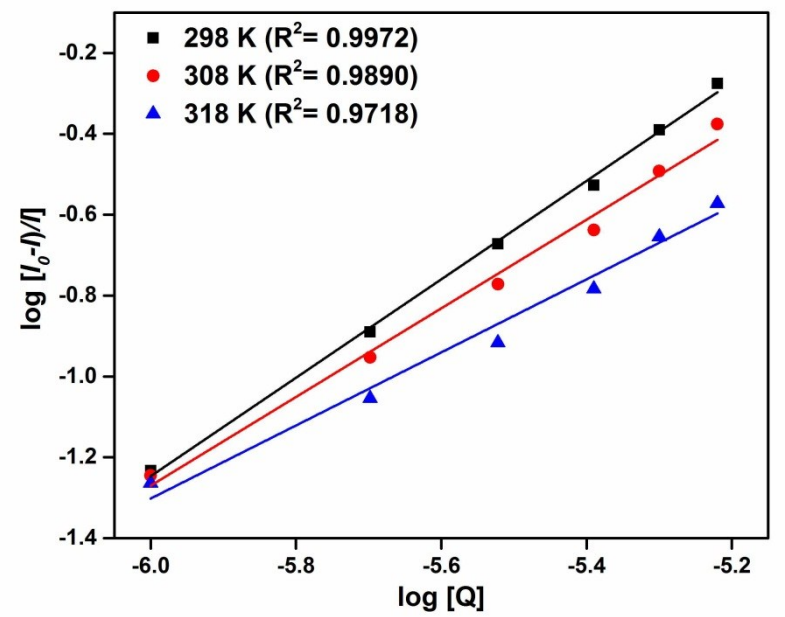

Figure S55. log[(I_0-I)/I] vs log[Q] plot at different temperatures.

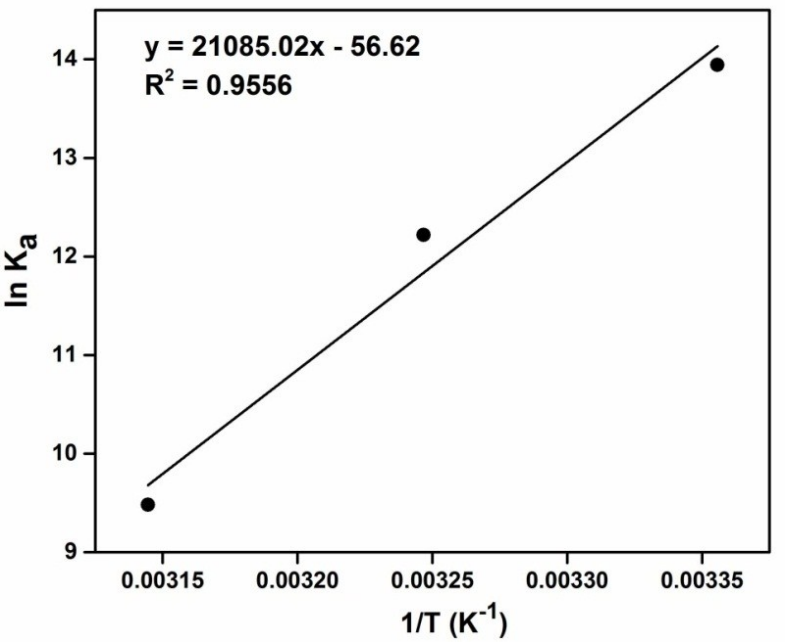

Figure S56. van't Hoff plot for the interactions between **1-NH_2@THB** and bilirubin.

Table S2. Comparison of the results of various bilirubin sensors.

A.	Fluorescent sensors						
Sl. No.	Sensor Material	Type of Material	Medium Used	Response Time (s)	Linear Range (M)	Detection Limit	Ref.
1	Al-MIL-53-NH_2@THB	MOF	HEPES buffer	30	10^{-12} – 1.2×10^{-5}	1.26 pM	This work
2	UIO-66-PSM	MOF	PBS buffer	30	10^{-13} - 5×10^{-4}	0.59 pM	1
3	PDPPF-*co*-Ph	polymer	THF	-	10^{-6} - 10^{-5}	-	2
4	BAMD	organic molecule	phosphate buffer	600	10^{-12} - 5×10^{-4}	2.8 pM (pH=7.4) 3.3 pM (pH=9.0)	3
5	PF-Ph-GlcA	polymer	PBS buffer	-	-	150 nm	4
6	HSA-AuNCs	nanoclusters	phosphate buffer	-	10^{-6} - 5×10^{-5}	248 nM	5

B.	Electrochemical sensors				
Sl. No.	Sensor Material	Type of Material	Linear Range	Detection Limit	Ref.
7	SiO_2@ZrONPs/ CHIT	nanoparticles	0.02- 250 µM	0.1 nM	6
8	CuO-CdO NCs	nanocomposite	10.0 pM -10.0 mM	1.0 ± 0.1 pM	7
9	HSA-AuNCs	nanomaterial	0.2-7.0µM	86.32 nM	8
10	BOx/nano Au	nanorods	0.01 -500 µM	0.005 µM	9
11	RGO-PSS composite electrode	carbon electrode	0 - 450 µM	2.0 µM	10
12	BOx/GONP@Ppy/FTO	graphene oxide nanoparticle	0.01 – 500 mM	0.1 nM	11
13	MWCNT	nanotubes	0.5–500 µM	0.3 ± 0.022 nM	12

References:

1. Y. Du, X. Li, X. Lv and Q. Jia, *ACS Appl. Mater. Interfaces*, 2017, **9**, 30925-30932.
2. T. Senthilkumar and S. K. Asha, *Macromolecules*, 2013, **46**, 2159−2171.
3. S. Ellairaja, K. Shenbagavalli, S. Ponmariappan and V. S. Vasantha, *Biosens. Bioelectron.*, 2017, **91**, 82-88.
4. T. Senthilkumar and S. K. Asha, *Macromolecules*, 2015, **48**, 3449-3461.
5. M. Santhosh, S. R. Chinnadayyala, A. Kakoti and P. Goswami, *Biosens. Bioelectron.*, 2014, **59**, 370-376.

6. B. Batra, S. Lata, Sunny, J. S. Rana and C. S. Pundir, *Biosens. Bioelectron.*, 2013, **44**, 64-69.
7. M. M. Rahmana, M. M. Hussain and A. M. Asiri, *Prog. Nat. Sci.: Mater. Int.*, 2017, **27**, 566-573.
8. M. Santhosh, S. R. Chinnadayyala, N. K. Singh and P. Goswami, *Bioelectrochemistry*, 2016, **111**, 7-14.
9. J. Narang, N. Chauhan, A. Mathur, V. Chaturvedi and C. S. Pundir, *Adv. Mater. Lett.*, 2015, **6**, 1012-1017.
10. T. Balamurugan and S. Berchmans, *RSC Adv.*, 2015, **5**, 50470-50477
11. N. Chauhan, R. Rawal, V. Hooda and U. Jain, *RSC Adv.*, 2016, **6**, 63624-63633.
12. M. Thangamuthu, W. E. Gabriel, C. Santschi and O. J. F. Martin, *Sensors*, 2018, **18**, E800.